Photochemical & Photobiological Sciences

PERSPECTIVE

Cite this: *Photochem. Photobiol. Sci.*, 2018, **17**, 1651

Mesoporous silica nanoparticles in recent photodynamic therapy applications

Sumeyra Bayir,[a,c] Alexandre Barras,[b] Rabah Boukherroub,[b] Sabine Szunerits,[b] Laurence Raehm,[a] Sébastien Richeter[a] and Jean-Olivier Durand *[a]

Received 5th April 2018,
Accepted 2nd July 2018

DOI: 10.1039/c8pp00143j

rsc.li/pps

In this review, the use of mesoporous silica nanoparticles for photodynamic therapy (PDT) applications is described for the year 2017. Since the pioneering work in 2009, nanosystems involving mesoporous silica nanoparticles have gained in complexity with a sophisticated core–shell system able to perform multi-imaging and multi-therapies, not only for cancer diseases but also for anti-microbial therapy, atherosclerosis, or Alzheimer disease. Near-infrared, excitation light based on up-converting systems, X-rays or persistent luminescent systems are described for deeper tissue treatments.

1. Introduction

Mesoporous silica nanoparticles (MSNs) have emerged as new and promising vectors for biological applications.[1–19] Since their first synthesis in 2001, around 3000 studies have been published dealing with MSNs, based on SciFinder. Their tunable diameter and pore size, easy functionalization,[20–23] and biocompatibility[24–26] allowed building efficient complex nanostructures[27] compared to other kinds of nanoparticles. Ligands can be readily attached onto their surface,[28,29] and stimuli-responsive (pH, redox, light, heat...) gatekeepers[30–38] can be integrated to avoid premature release of the payload and to deliver the active agent exclusively at the diseased site. MSNs functionalized with photosensitizers (PS) are also of great interest for photodynamic therapy (PDT). PDT is a form of treatment that administers orally or intravenously photosensitizing agents, which concentrate in certain cells, followed by exposure of the tissue to light, in order to destroy abnormal tissue.[39,40] When photosensitizers are exposed to a specific wavelength of light, reactive oxygen species (ROS), in particular singlet oxygen, known for their cytotoxic nature, are produced. PDT can be applied for the treatment of various diseases including cancer cell ablation as well as for the treatement of infections. To enhance the selectivity towards tumor cells and the efficiency of PDT, photosensitizer encapsulation in nanoparticles is a promising method that has gained tremendous focus. Many nanoparticulate vectors have been proposed for PDT, one of them being silica-based nanostructures.[41–49] MSNs were proposed for the first time as highly promising vectors for PDT in 2009. The photosensitizers used were porphyrins integrated either inside the MSN pores[50,51] or into the MSN walls.[52] Vectorization could be achieved using ligands such as mannose[52] or RGD peptides[53] and used for anti-tumor applications. Since then, the field expanded largely and was recently reviewed showing the biocompatibility of MSNs.[54] Core shell and more elaborated nanostructure-based MSNs have been designed for theranostic applications. In the present review, we highlight the most recent progess made concerning the use of different MSN derivatives for efficient PDT.

2. Photodynamic therapy (PDT) using mesoporous silica nanoparticles

A common feature of most tumors is a low level of oxygen, called hypoxia.[55] Tumor hypoxia is known to be associated with radio/chemo-resistance and metastasis that eventually lead to cancer progression. It prevents the sucess of cancer therapies such as chemotherapy, radiotherapy and PDT. Kim *et al.* developed biocompatible manganese ferrite (MF, $MnFe_2O_4$) nanoparticles of 6 nm diameter conjugated to 50 nm-sized mesoporous silica nanoparticles (MFMSNs) in order to improve the therapeutic effects of PDT against hypoxia.[56] Manganese ferrite nanoparticles (MFNs) are Fenton catalysts, continously decomposing hydrogen peroxide (H_2O_2) into O_2 and H_2O. With hydrogen peroxide being an abundant metabolite produced in an hypoxic microenvironment the presence of MFNs can counterbalance the oxygen loss by producing O_2 (Fig. 1). After attachment of MFNs to MSNs, the

[a]*Institut Charles Gerhardt Montpellier, UMR 5253, CNRS-UM-ENSCM, Université de Montpellier, Place Eugène Bataillon 34095, Montpellier cedex 05, France. E-mail: durand@umontpellier.fr*
[b]*Univ. Lille, CNRS, Centrale Lille, ISEN, Univ. Valenciennes, UMR 8520 – IEMN, F-59000 Lille, France*
[c]*Department of Chemistry, Gebze Technical University, Kocaeli 41400, Turkey*

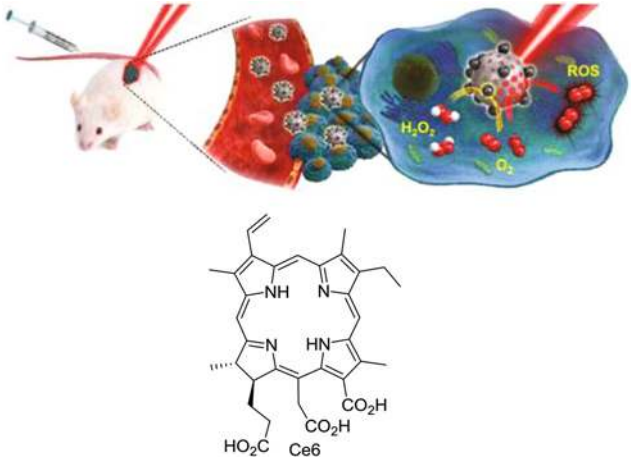

Fig. 1 Schematic illustration of the use of Ce6 and manganese ferrite (MF) loaded mesoporous silica nanoparticles (MFMSN). Reprinted with permission of ref. 56. Copyright 2017 American Chemical Society.

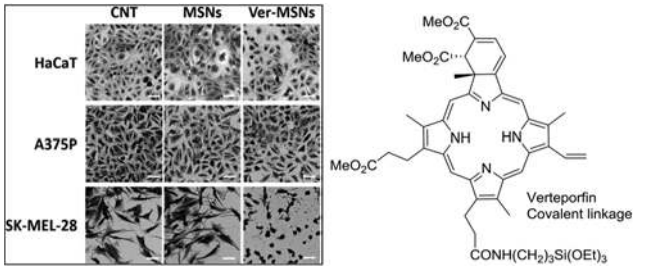

Fig. 2 PDT effects on cell proliferation of three different cell lines, control, MSNs and verteporfin modified MSNs. Optical microscopy images magnification = 10×. CNT = control, MSNs (10 μg mL^{-1}), Ver-MSNs (10 μg mL^{-1}). Reprinted from ref. 57, with permission from Elsevier.

high Brunauer–Emmett–Teller (BET) surface area of 429.4 m^2 g^{-1} with a pore size of 2.8 nm allowed a high loading of the photosensitizer Ce6. Functionalization was made with polyethylene glycol (PEG) to prevent nonspecific protein binding and enable passive targeting *via* the EPR effect. MFMSNs showed high r_2 relaxivity suitable for use as a magnetic resonance imaging (MRI) contrast agent. Using U-87 MG cells incubated with a hypoxic medium (1% O_2, 5% CO_2, and 94% N_2) for a few hours, the degree of hypoxia could be determined by monitoring hypoxia-inducible factor (HIF-1α) levels, upregulated under hypoxic conditions.

Western blot assays showed that the HIF-1α signal intensity decreased when the concentration of MFMSN-Ce6 increased. Furthermore, MFMSN-Ce6 generated 2 times more ROS under hypoxia than Ce6 alone, as determined by singlet oxygen sensor green (SOSG) experiments. PDT was then carried out under hypoxic conditions using U-87 MG cells. The group also examined PDT *in vivo* with xenografted solid tumors of U-87 MG cells in BALB/c nude mice. After intravenous injection, MFMSNs accumulated in the tumor by the EPR effect as shown by MRI. Using immunohistochemistry (IHC) to monitor HIF-1α levels, it was found that after MFMSN treatment, down-regulation of HIF-1α occured due to the production of a substantial level of oxygen at a low H_2O_2 concentration under hypoxia *in vivo*.

Another important example is the treatment of malignant melanoma, considered as the most risky type of skin cancer in terms of epidemiology, increasing two-fold every 10–20 years worldwide. The increase in melanoma is simply driven by populations that are both growing and aging. Surgery is generally used to treat skin cancer, with PDT being very promising for melanoma therapy. Rizzi and coworkers coupled aminopropyltriethoxysilane modified MSNs with verteporfin (Ver) through amide bond formation. The obtained nanosystem (Ver-MSNs) was examined using an *in vitro* model for PDT of melanoma (Fig. 2).[57] SK-MEL-28 cell line irradiation with red light resulted in nearly 70% decrease in cell growth after 180 s exposure as monitored using optical microscopy. In contrast to the control and MSNs, Ver-MSN based PDT provided a significant morphological change in SK-MEL-28 cells, a high metastatic melanoma cell line (Fig. 2) by significantly reducing cell proliferation. Ver-MSNs could therefore offer a PDT anti-tumor modality for quite invasive melanoma.

Wong *et al.* used covalent linking to immobilize zinc(II) phthalocyanine (ZnPc) dimer to MSNs.[58] Two strategies have been adopted in this work using (i) acid-cleavable (cPc) and non acid-cleavable (nPc) linkers (Fig. 3). Inside the mesopores, the dimeric ZnPc showed weak fluorescence emission and $^1O_2$ generation both in *N*,*N*-dimethylformamide and PBS due to the self-quenching effect, compared to the free molecular counterparts. In contrast, the singlet oxygen generation efficiency, as reflected by the rate of photodegradation of 1,3-diphenylisobenzofuran (DPBF), increased at lower pH for cPc@MSN, but not for nPc@MSN, over the pH range 5.5–7.4, demonstrating the pH-responsive photosensitizing property of cPc@MSN. Interestingly, the $^1O_2$ generation efficiency of cPc@MSN was comparable to that of monomeric ZnPc (mPc) after 24 h at pH 5.5.

The cytotoxicity of cPc@MSN and nPc@MSN was examined on human colon adenocarcinoma HT29 cells using the classical MTT assay. While both nanosystems were not cytotoxic in the absence of light, cPc@MSN was highly potent under visible light irradiation (610 nm, 40 mW cm^{-2}, 48 J cm^{-2}) with an IC_{50} value of 31 nM, comparable to 46 nM recorded for free cPc. The nPc@MSN remained non-photocytotoxic in the concentration range tested. *In vivo* studies on a HT29 xenograft in Balb/c nude mice treated with an intratumoral dose of cPc@MSN or nPc@MSN (equivalent to 40 nmol of cPc or nPc per kg body weight) revealed that the intratumoral fluorescence intensity increased gradually over 24 h for cPc@MSN, while it remained very weak for nPc@MSN. The results suggest that cPc@MSN can be potentially used as an activatable photosensitizing agent for PDT.

To enhance the therapeutic effect and minimize systemic toxicity, Yuan *et al.* developed redox-responsive photodynamic MSNs through incorporation of protoporphyrin IX (PpIX) and

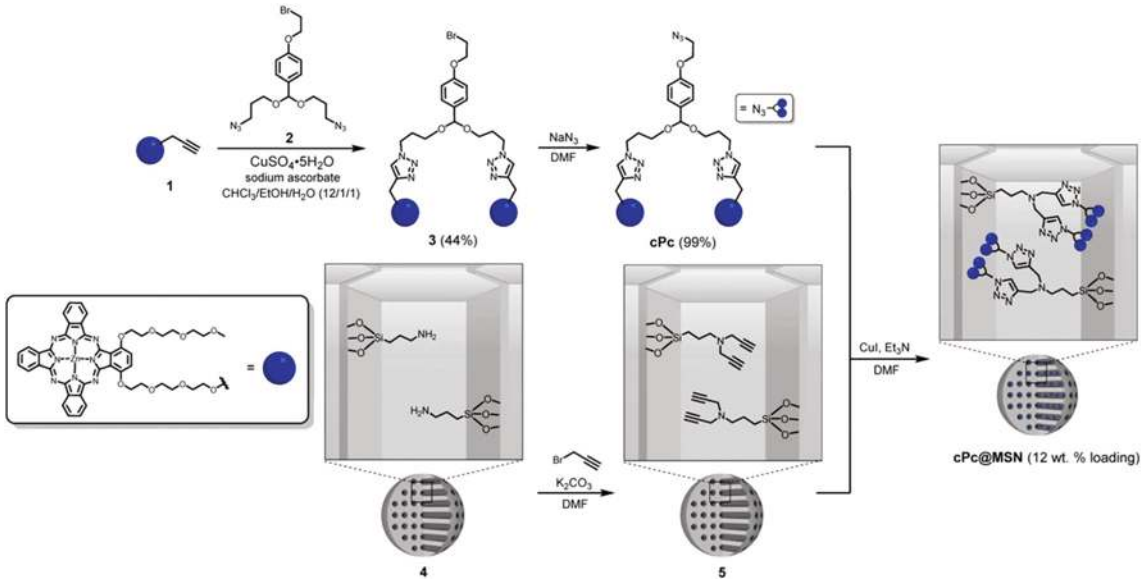

Fig. 3 Synthesis of zinc(II) phthalocyanine dimer immobilized through an acid-cleavable linker to MSNs using "click" chemistry. Reprinted with permission from ref. 58. Copyright 2017 American Chemical Society.

multifunctional peptides, BHQ-MSN-SS-PpIX&RGD.[59] The synthetic route is illustrated in Fig. 4. RGD peptide was incorporated to achieve tumor cell targeting, given that the strong interaction of the tumour-targeted peptide sequence RGD with the $\alpha_v\beta_3$ integrin receptor (overexpressed on tumour cells) is well-established. PpIX was modified with a PEG linker to enhance its long circulating property, while the presence of the S–S bond allows effective release of the PpIX inside the cells by bond breaking by excess glutathione (GSH) present in tumour cells. The active targeting ability of BHQ-MSN-SS-PpIX&RGD for integrin-positive tumour cells was confirmed by confocal laser scanning microscopy (CLSM) using HeLa cells (cervical cancer cells). HeLa cells incubated with BHQ-MSN-SS-PpIX&RGD displayed obviously red fluorescence, indicating PpIX fluorescence recovery. This is in contrast to HeLa cells pre-treated with free RGD. The data suggest that, by blocking the $\alpha_v\beta_3$ integrin receptor with free RGD, the cellular uptake of nanoparticles in the HeLa cells was inhibited.

The PDT efficacy of BHQ-MSN-SS-PpIX&RGD under visible light irradiation was assessed *in vitro* on HeLa cells using the MTT assay. Without irradiation, BHQ-MSN-SS-PpIX&RGD exhibited low cytotoxicity on the tumour SCC-7 and HeLa cells, and the normal COS7 cells. Upon 30 min visible light irradiation, the cell viabilities of the tumour cells were much lower than

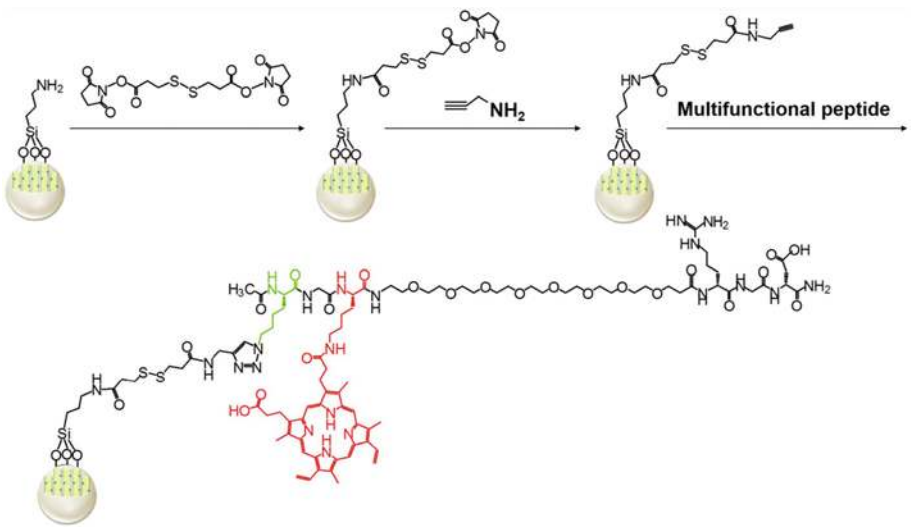

Fig. 4 Synthesis of of MSNs BHQ-MSN-SS-PpIX&RGD nanostructures. Reproduced from ref. 59 with permission from the Royal Society of Chemistry.

that of the normal cells under otherwise identical conditions, indicating specific targeting of the tumour cells. The half-inhibitory concentration (IC_{50}) of BHQ-MSN-SS-PpIX&RGD under visible light irradiation was 85 μg mL^{-1} for HeLa cells.

Although the first generation of photosensitizers (PS), mainly based on porphyrins, has shown to be efficient in the treatment of many cancer types, it has disadvantages, related to their low absorption of light and poor light penetration into the tumor due to the relatively short wavelength absorption. These drawbacks can be overcome by the use of PS that can be activated in the NIR (700–980 nm) spectrum of light. Miletto *et al.*[60] integrated different brominated squaraine based dyes (Br-NH, Br-C2, Br-C4) (Fig. 5) onto MSNs by pre-treating the particles at 100 °C overnight followed by simple impregnation at room temperature and assessed the $^1O_2$ release ability of the three MSN platforms using 1,3-diphenylisobenzofuran (DPBF) in solution upon irradiation at 630 nm (450 W xenon lamp). The Br-NH/MSN nanoplatform was found to be more effective in $^1O_2$ generation compared to Br-C2/MSN and Br-C4/MSN. Based on the spectroscopic data and theoretical investigation, it was suggested that Br-NH is homogeneously distributed on the MSN, while the other squaraine molecules experienced aggregation. Even though this study was limited to the solution phase behaviour of squaraine/MSN nanoplatforms, it provides valuable physico-chemical data on how PS adsorption on MSNs affects $^1O_2$ generation, which represents an important step for PDT applications.

3. Upconverting nanoparticle (UCNP)-based MSNs

A new generation of luminophores, also termed upconversion nanoparticles (UCNPs), has the ability to convert near infrared radiation with lower energy into visible radiation with higher energy *via* a nonlinear optical process.[61] UCNPs have thus been considered as alternative fluorescent labels, showing great potential for imaging and biodetection assays both *in vitro* and *in vivo*. These particles have also found interest in PDT. The group of Han described mesoporous-silica-coated upconverting nanoparticles loaded with photosensitizers for PDT.[62] Ultrathin mesoporous silica shell (12 ± 2 nm thickness) coated UCNP particles ($NaYF_4$:Yb/Er/Nd@$NaYF_4$:Nd) called UCNP@$mSiO_2$(CTAB) (Fig. 6) were functionalized with aminopropyltriethoxysilane in order to covalently link the carboxyl groups of 1-adamantane carboxylic acid (AD-COOH). CTAB was removed and the free channels functionalized with aminopropyltriethoxysilane, so that the inner channels of the UCNP@$mSiO_2$-AD become positively charged allowing the integration of negatively charged Rose Bengal (RB) very rapidly (2 min). A hydrophilic host molecule, β-cyclodextrin (CD), was coated onto the surface of RB-NH_2-UCNP@$mSiO_2$-AD through inclusion with the guest AD to further block the pores and to stabilize the nanoparticles in biological media, leading to RB-NH_2-UCNP@$mSiO_2$-AD-CD. The nanoparticles did not show any significant cytotoxicity on HeLa cells without NIR irradiation. The *in vitro* PDT effect of RB-NH_2-UCNP@$mSiO_2$-

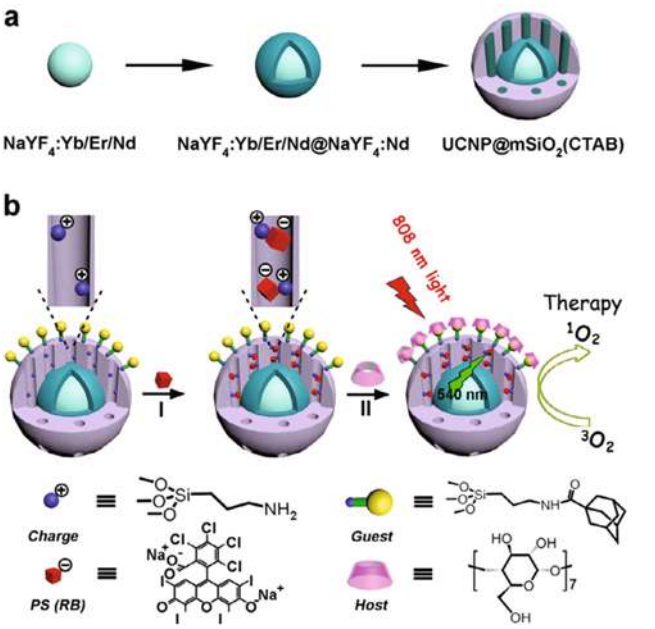

Fig. 6 (a) Schematic diagram for the synthesis of UCNP@m-SiO_2(CTAB). (b) Schematic illustration of the preparation of RB-NH_2-UCNP@$mSiO_2$-AD by functionalization (Process I), and 808 NIR-light-triggered $^1O_2$ generation after β-CD surface capping (RB-NH_2-UCNP@$mSiO_2$-AD-CD) (Process II). Reproduced with permission from ref. 62, Copyright 2017 Wiley-VCH Verlag GmbH & Co. KGaA, Weinheim.

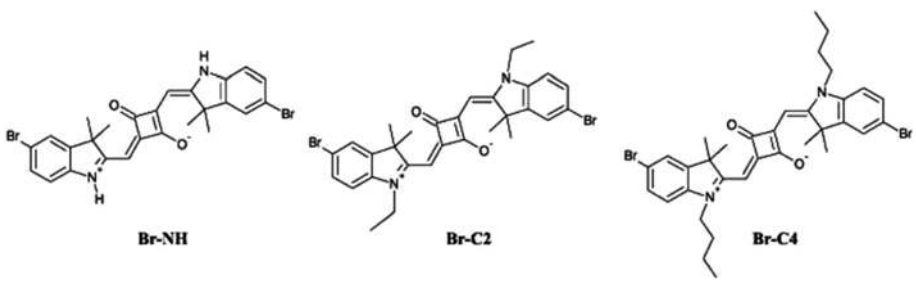

Fig. 5 Chemical structure of different squaraine derivatives adsorbed onto MSNs. Reproduced from ref. 60 with permission from the Royal Society of Chemistry.

AD-CD nanoparticles upon 808 nm NIR light irradiation was examined as a function of irradiation time, power density, and concentration and these parameters were optimized in order to lead to very efficient NIR PDT. Note that 808 nm NIR light was much safer than commonly used 980 nm NIR light, which leads to an overheating effect.

Wang *et al.* designed a novel modality for deactivation and detection of vulnerable atherosclerosis plaques based on a UCNP ($NaYF_4$:Yb/Er) core with a uniform shell of 28 ± 1 nm thick mesoporous silica shell (Fig. 7) to which Ce6 was loaded forming UCNP@mSiO_2-Ce6.[63] Atherosclerosis (AS) is a common chronic inflammatory vascular disorder, seen in clinical patients which represents a serious health problem of people. Macrophages constitute 20% of the cells in atherosclerotic lesions. They are in a critical position for the atherosclerosis development and the ruptured unstable plaque development which form during atherosclerosis. Although the mechanical endovascular techniques reduced the deaths from this disease, they include restenosis owing to intimal hyperplasia or constrictive remodeling. The *in vitro* test proved that UCNP@mSiO_2-Ce6 could induce the apoptosis of THP-1 macrophages and 40% cell death at 16 μg mL^{-1} nanoparticle concentration and 60 s laser irradiation time (power density 1.8 W cm^{-2}), which confirmed that NIR PDT with UCNP@mSiO_2-Ce6 was efficient and could be used for atherosclerosis theranostics.

Kuk *et al.* have shown the application of $NaYF_4$ based UCNPs co-doped with Yb/Er and coated with a rattle-structured phenylene based organosilica (ROS)-shell as a therapeutic platform for Alzheimer's disease, a neurodegenerative disorder (Fig. 8).[64] The pathological characteristic of Alzheimer's disease is the excessive generation and aggregation of the

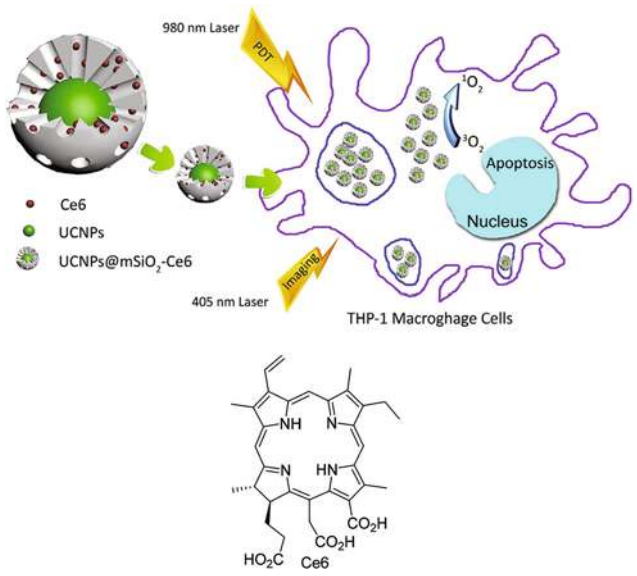

Fig. 7 Schematic illustration of NIR activated upconversion PDT and photosensitizer-based downconversion imaging for THP-1 macrophage using UCNPs@mSiO_2-Ce6 nanoparticles. Reprinted from ref. 63, with permission from Elsevier.

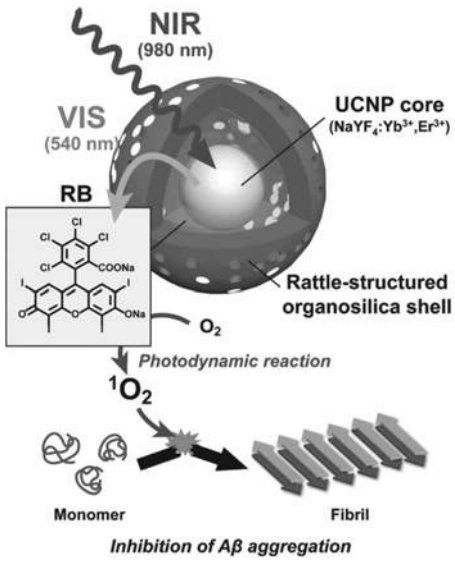

Fig. 8 Schematic illustration of β-amyloid aggregation inhibition by NIR-mediated rattle structured UCNPs loaded with RB. Reproduced with permission from ref. 64, Copyright 2017 Wiley-VCH Verlag GmbH & Co. KGaA, Weinheim.

β-amyloid (Aβ) peptide in the brain. The method is based on the NIR-light-induced suppression of Aβ aggregation utilizing Rose Bengal (RB) as a photosensitizer. The circular dichroism (CD) spectrum of non-treated Aβ peptides demonstrates a β-sheet-rich protein structure, which has positive and negative bands at 195 nm and 216 nm, respectively, representing the assembly of Aβ monomers into fibrils. According to the CD spectrum two active peaks of β-sheets definitely disappeared when Aβ monomers were incubated with RB/UCNP@ROS upon NIR light irradiation. Aβ aggregation was efficiently suppressed by RB-loaded core/shell upconverting nanoparticles and photosensitization upon 980 nm NIR light irradiation. Furthermore, Aβ peptides incubated for 24 h with PC12 Cells indicated a high toxicity of the Aβ aggregates. When PC12 cells were incubated with Aβ peptide solution previously treated with PDT, the solution was not toxic. Therefore RB/UCNP@ROS was biocompatible and efficient in preventing the Aβ-induced cytotoxicity upon NIR light irradiation. The results showed that the combination of RB/UCNP@ROS and NIR light is promising for the development of PDT for Alzheimer's disease.

Another example is that of Xu *et al.*, who used yolk-structured multifunctional up-conversion nanoparticles (UCNPs) that combine photodynamic and sonodynamic therapy to eradicate antibiotic resistant bacteria.[65] A multi-step process was used to synthesize the multi-functional UCNP@SiO_2-RB/HMME nanoparticles (Fig. 9).

Given that both sonodynamic therapy (SDT) and PDT are based on PS activation and $^1O_2$ generation, the activity of UCNP@SiO_2-RB/HMME NPs for $^1O_2$ production was investigated under various conditions, each mimicking SDT, PDT or a combination of both. NIR irradiation or ultrasonic treatment

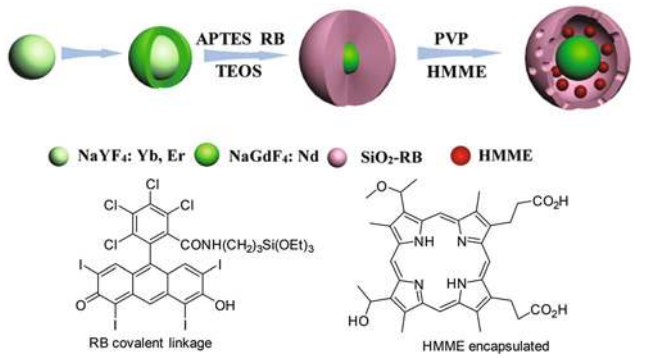

Fig. 9 Illustration of the different steps for the synthesis of UCNP@SiO_2-RB/HMME NPs. Reproduced from ref. 65 with permission from the Royal Society of Chemistry.

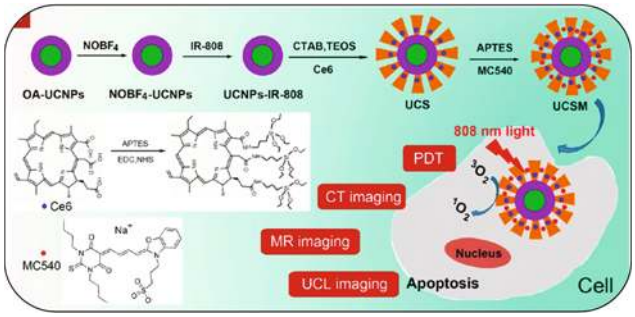

Fig. 10 Functionalization of dye-sensitized UCNPs with mesoporous silica and the dual-photosensitizer Ce6 and MC540 for imaging-guided PDT. Reprinted with permission from ref. 66. Copyright 2017 American Chemical Society.

of a DPBF solution in the absence of UCNP@SiO_2-RB/HMME NPs was not able to generate $^1O_2$. In contrast, the 980 nm irradiation or 20 min ultrasonication of a DPBF solution in the presence of UCNP@SiO_2-RB/HMME NPs led to a decrease of DPBP absorption to 50% and 41%, respectively. The DPBF absorption decreased even further to reach 12% when a sequential treatment consisting of 980 nm irradiation and 20 min ultrasonication was performed. The efficacy of UCNP@SiO_2-RB/HMME NPs against drug-resistant Gram-positive MRSA and Gram-negative ESBL-producing *E. coli* was assessed under NIR irradiation, ultrasonic treatment or the combination of the two modalities. While the application of a single modality did not lead to complete bacteria eradication (74.2% for PDT and 70% for SDT), treatment using a dual modality (PDT + SDT) led to 100% bacteria killing using 125 μg mL^{-1} of UCNP@SiO_2-RB/HMME NPs, a concentration that was not toxic to both bacterial strains under dark conditions.

Independently, Xu *et al.* prepared IR-808-sensitized up-conversion nanoparticles ($NaGdF_4$:Yb,Er@$NaGdF_4$:Nd,Yb) coated with mesoporous silica loaded with Ce6 (red-light-excited photosensitizer) and MC540 (green-light-excited photosensitizer) through covalent bonding and electrostatic interactions, respectively (Fig. 10).[66] The nanoparticles were biocompatible for concentrations up to 500 μg mL^{-1}. Interestingly, the presence of Gd^{3+} in the NPs was beneficial to realize MRI, while Yb element enhanced the CT imaging capability of the material. The *in vitro* PDT efficacy of the nanoparticles was examined on HeLa cells. While direct 808 nm irradiation of the cells did not show any apparent cell killing (decrease of cell viability), incubation with the nanoparticles followed by 808 nm irradiation led to effective cell killing. It is important to note that 980 nm laser-irradiation had a lower cell-killing efficacy than that at 808 nm. The *in vivo* efficacy of the synthesized nanoparticles was evaluated on U14 tumour-bearing mice under 808 nm irradiation, by recording the body weight and tumour size every 2 days during two weeks after the initial treatment. No body weight loss was observed using the nanoparticles or their components, suggesting that the samples have no adverse drug reaction or side effects on the mice. More importantly, the mice treated with the nanoparticles and irradiated with a NIR laser exhibited the highest tumour inhibition efficiency, along with the highest level of tissue damage as revealed by the histological studies.

Another therapeutic agent based on enzyme and pH-responsive nanocarriers was reported lately.[67] This 75 nm size nanoplatform comprises an up-conversion nanoparticle (UCNP, $NaYF_4$:Yb,Er@$NaYF_4$) core and a mesoporous silica shell loaded with embedded chlorine e6 (Ce6) (UCNP@mSiO_2-Ce6). The nanoparticles were functionalized with the sensitive succinic acid–glycine–phenylalanine–leucine–glycine (SGFLG) linker to encapsulate an anticancer drug (DOX). The targeting property of the nanoplatform was ensured through modification with transferrin (Tf) owing to the overexpression of Tf receptors (TfR) in tumour cells (Fig. 11). Inside the cells, drug release can be initiated by the presence of a high concentration of cathepsin B and low pH through SGFLG "gate" opening. Furthermore, under NIR (980 nm, 0.5 W cm^{-2}) irradiation, the UCNPs emit visible light able to excite Ce6 to generate ROS and achieve PDT. The DOX release from UCNP@mSiO_2/Ce6–DOX–SGFLG2 was investigated for different concentrations of cathepsin B in PBS (pH 6.8). It was observed that cathepsin at a concentration of 2×10^7 mol L^{-1} induced up to 60.17% DOX release, while a lower concentration ($<2 \times 10^8$ mol L^{-1}) of cathespsin showed a limited (23.86%) DOX release.

Similarly, DOX release from UCNP@mSiO_2/Ce6–DOX–SGFLG2 was pH-dependent (in the absence of cathepsin B) with drug release levels reaching 52.37% at pH 5.0, 70.41% at pH 3, and 78.36% at pH 1.2. The pH-dependence drug release was ascribed to amide breaking in the SGFLG linker under acidic conditions.

The cell viability was investigated on tumour cancer cells (HeLa) and normal human liver cells (L02) incubated with UCNP@mSiO_2/Ce6–SGFLG–Tf and UCNP@mSiO_2/Ce6–DOX–SGFLG–Tf in the concentration range of 0–500 μg mL^{-1} using the MTT assay. Both L02 and HeLa cell lines exhibited negligible reduced cell viability for UCNP@mSiO_2/Ce6–SGFLG–Tf (~95%) even for the highest concentration (500 μg mL^{-1})

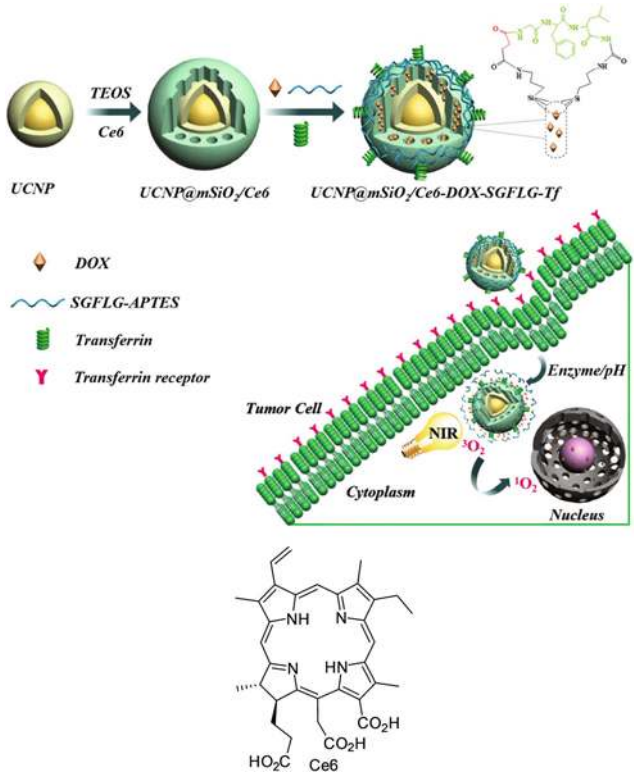

Fig. 11 Schematic illustration of the synthesis of UCNP@mSiO$_2$/Ce6–DOX–SGFLG–Tf and enzyme/pH induced release process. Reproduced from ref. 67 with permission from the Royal Society of Chemistry.

studied, indicating the good biocompatibility of the nanocarrier. A different behaviour was observed for HeLa cells incubated with UCNP@mSiO$_2$/Ce6–DOX–SGFLG–Tf; a decrease of cell viability to 53% was recorded due most likely to the excess expression of cathepsin B in this cell line. For the normal L02 cells, a high cell viability (~92%) was attained. Upon 980 nm irradiation for 5 min of HeLa cells incubated with UCNP@mSiO$_2$/Ce6–DOX–SGFLG–Tf, the cell viability decreased to 45%, indicating the synergistic effect of chemotherapy and PDT. By increasing the irradiation time to 15 min, the cell viability decreased further to 33%. The enhanced nanoparticle uptake by HeLa cells was evidenced by fluorescence imaging.

4. Persistent-luminescent nanoparticles (PLNPs)

Many of the porphyrin-based PSs exhibit excitation wavelengths in the UV-Visible spectrum. Continuous exposure of living cells and tissues to UV-blue light can lead to DNA damage and cell killing. Wang *et al.* proposed novel persistent-luminescent nanoparticles (PLNPs), which cause effective cancer cell destruction upon low-dose UV light applied by fragmented irradiation, and therefore the side-effects arising from prolonged UV irradiation could be reduced.[68] They designed phosphorescent $Zn_{1.25}Ga_{1.5}Ge_{0.25}O_4$:0.5%$Cr^{3+}$,2.5%$Yb^{3+}$, and 0.25%$Er^{3+}$ triple-doped (TD-ZGGO) nanoparticles by co-adjusting the Ge, Cr^{3+}, Yb^{3+}, and Er^{3+} loadings in the matrix (Fig. 12).

Mesoporous silica coated TD-ZGGO nanoparticles demonstrated important fluorescence emission, long afterglow luminescence, monodisperse nanoparticle size distribution, minimum toxicity, and high biocompatibility with HeLa cells. TD-ZGGO@mSiO$_2$ persistent luminescent nanoplatforms were loaded in the pores of the amino-functionalized mesoporous silica shell with sulfonated aluminum phthalocyanine (AlPcS) through electrostatic interactions. A significant amount of singlet oxygen was produced by AlPcS *via* the FRET system. With the afterglow luminescence of TD-ZGGO nanoparticles, the FRET process can substantially minimize the UV light dosage utilized to activate the conjugated PS for PDT applications. Therefore, HeLa cell necrosis and apoptosis were evaluated through laser scanning confocal microscopy (LSCM) and flow cytometry after incubation with TD-ZGGO@mSiO$_2$-AlPcS. The cancer cell killing effect was improved for a cumulative light dose (8 J cm^{-2}) with fractioned light irradiation. The PS-conjugated PLNPs displayed an important enhanced cancer cell destruction feature.

5. Other MSNs used for PDT

PDT is inadequate for the treatment of tumors in internal organs. To overcome this limitation, X-PDT technology has

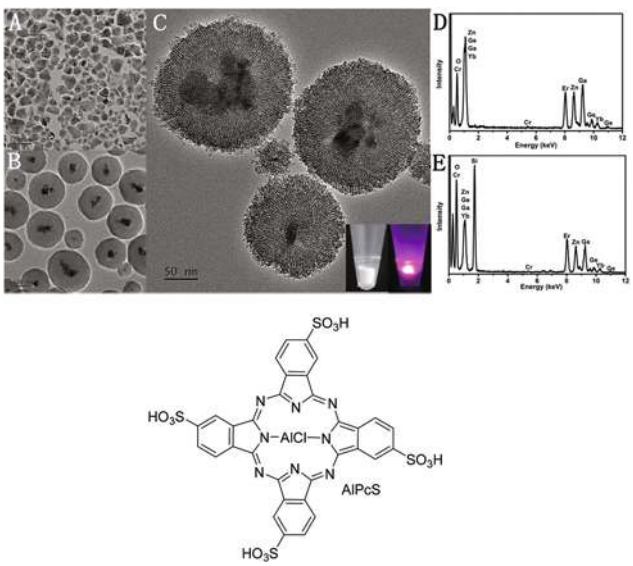

Fig. 12 Physical characteristics of TD-ZGGO nanoparticles. (A) TEM image of bare TD-ZGGO nanoparticles. (B and C) TEM images of TD-ZGGO@mSiO$_2$ at relatively low (B) and high (C) magnifications. The lower-right inset in (C) presents the fluorescence of TD-ZGGO@mSiO$_2$ under 405 nm irradiation. (D and E) EDX spectroscopy patterns of TD-ZGGO nanoparticles before (D) and after (E) coating with a mesoporous silica shell. Reproduced from ref. 68 with permission from the Royal Society of Chemistry.

been recently carried out. In this original approach, scintillator nanoparticles are used as transducers and X-rays can indirectly activate PDT. A study by Chen *et al.* used 2,3-naphthalocyanine (NC) and $LiGa_5O_8$:Cr(LGO:Cr) co-loaded mesoporous silica nanoparticles (NC-LGO:Cr@$mSiO_2$) as an original scintillator for effective X-PDT against non-small cell lung cancer (NSCLC).[69] The NC-LGO:Cr@$mSiO_2$ nanoparticles were mixed with singlet oxygen sensor green (SOSG) in order to calculate the singlet oxygen generation under X-rays. X-rays alone provided a small luminescence increase, however NC-LGO:Cr@$mSiO_2$ induced an important and time-dependent increase of fluorescence intensity, indicating efficient singlet oxygen generation through X-PDT. X-PDT demonstrated good efficacy with ~100 nm NC-LGO:Cr@$mSiO_2$. NC-LGO:Cr@$mSiO_2$ could effectively mediate X-PDT, generate singlet oxygen and destroy cancer cells. LGO:Cr emits strong persistent X-ray triggered optical luminescence (XEOL) in the NIR (~720 nm) efficiently allowing deep tissue detection. NC-LGO:Cr@$mSiO_2$ was conjugated with cetuximab (CTX) in order to target lung cancer. Therefore imaging-guided X-ray therapy was carried out *in vivo* in a lung orthotopic tumor model in mice (Fig. 13). Intravenous injection of NC-LGO:Cr@$mSiO_2$-CTX and X-PDT allowed efficient X-PDT, suggesting X-PDT as a new treatment modality.

The "always-on" type PDT agents have limitations such as nonspecific production of fluorescence and $^1O_2$, poor imaging contrast and long-term skin photosensitivity. To overcome such drawbacks, Hong *et al.* examined the design of "off-on" type PDT agents utilizing hollow mesoporous silica nanoparticles (HMSNPs) to allow an enhanced delivery of PSs to cancer cells and switchable optical features of the PSs.[70] Fluorescence and $^1O_2$ production remain "off" in the native state of HMSNPs due to FRET between the loaded photosensitizers. Using talaporfin sodium (TS), a second generation PDT agent as a PS model, the PSs could be released from the HMSNPs, subsequently turning "on" the fluorescence and singlet oxygen production (Fig. 14). The intercellular uptake of TS@HMSNPs and fluorescence turn-on *in vitro* were followed by confocal laser scanning microscopy. After 24 h of incubation with SCC-7 cancer cells, fluorescence imaging showed that the intercellular uptake of TS@HMSNPs was much better than free TS. Additionally, the uptake of TS@HMSNPs was 35.4 times higher compared to free TS. Under CW laser (670 nm) illumination, cancer cell viability was 20% with TS@HMSNPs, wheras free TS at 20 μM showed 82% viability. The high therapeutic efficacy of TS@HMSNPs to deliver TS molecules more effectively into the cancer cells is a result of

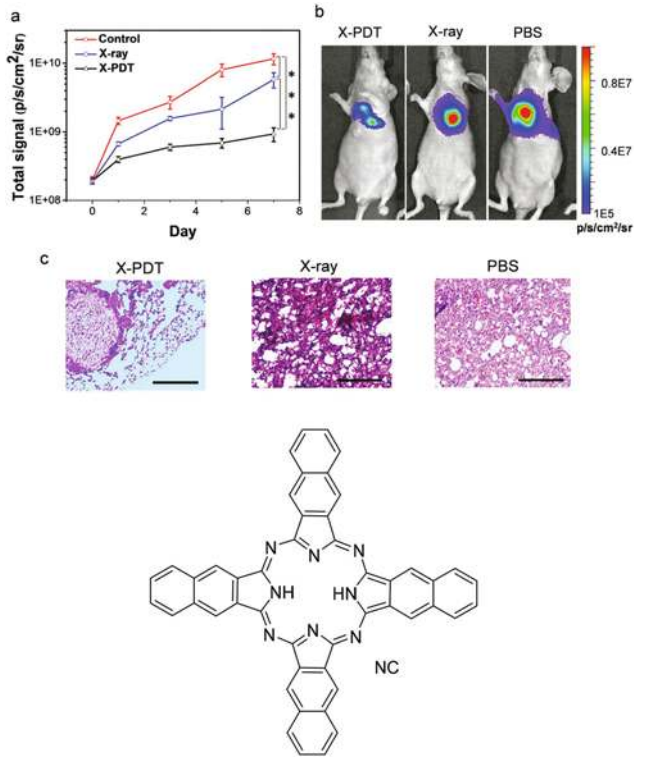

Fig. 13 *In vivo* therapy of X-PDT. (a) Tumor growth, assessed by monitoring BLI signal changes at different time points. Compared to irradiation alone, X-PDT suppressed much more efficiently tumor growth. $P < 0.001$. (b) Representative BLI images for the three treatment groups, taken on day 7. (c) H&E staining on tumor tissues. Compared to the control and irradiation alone, X-PDT effectively controls tumor generation in the lungs. Scale bars: 200 μm. Reproduced from ref. 69 with permission from the Royal Society of Chemistry.

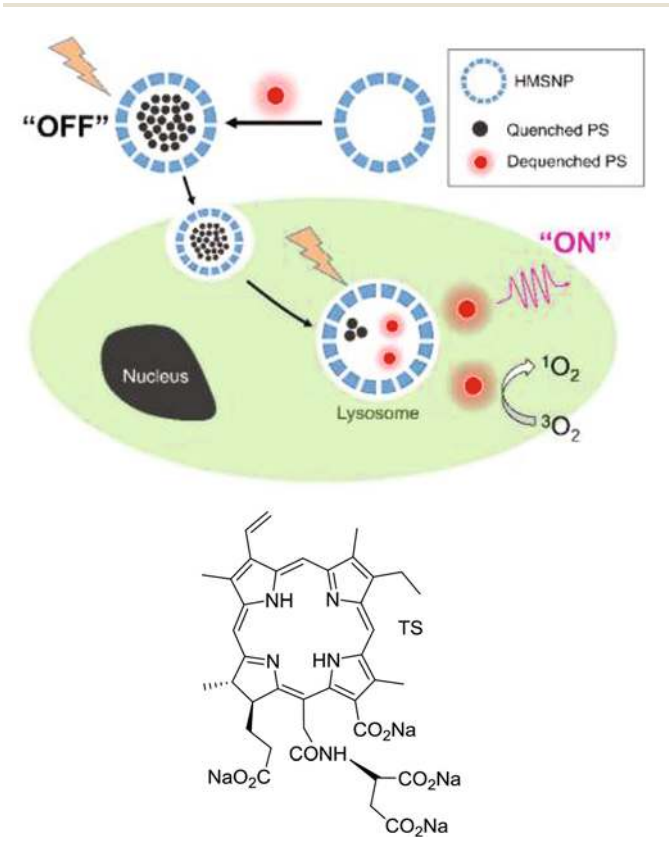

Fig. 14 Schematic diagram of the TS@HMSNP for activatable fluorescence imaging and PDT. Reproduced with permission from ref. 70, Copyright 2017 Wiley-VCH Verlag GmbH & Co. KGaA, Weinheim.

the cell lysate, as confirmed by fluorescence experiments. The TS@HMSNP composite demonstrated excellent capacity for selective fluorescence imaging and PDT of cancers.

The major issues of PDT agents are nonspecific fluorescence and $^1O_2$ production causing poor imaging contrast and severe side effects such as skin sensitivity, respectively. Indeed, developing activatable PDT agents are of great interest to solve these problems. In this context, Suk ho and coworkers[71] reported the synthesis of hollow mesoporous silica nanoparticles (HMSNPs) loaded with indocyanine green (ICG) as a photosensitizer. ICG is a water-soluble tricarbocyanine dye approved by FDA for clinical use, which has absorption and emission bands in the near-infrared range (NIR, 650–850 nm). It produces $^1O_2$ and heat upon NIR irradiation, but it also presents some important drawbacks: it is quite sensitive in aqueous solutions since it decomposes upon light irradiation and/or heat and it has a quite short half-life of a few minutes in blood limiting its bioavailability. The nanoparticles reported by Choi and coworkers (Fig. 15), namely ICG@HMSNPs, were obtained by loading ICG in preformed HMSNP and a subsequent PEGylation reaction. Around 177 mg of ICG could be loaded per g of HMSNPs. The obtained ICG@HMSNPs have a mean diameter of ~160 nm, a mean hydrodynamic radius of 227 nm, and a zeta-potential of 26.2 mV. Due to the fact that ICG molecules are aggregated within ICG@HMSNPs, the fluorescence intensity is quenched and 118 times lower than that of free ICG. At the same time, $^1O_2$ production is also completely turned off. *In vitro* studies on SCC-7 squamous carcinoma cells indicate that intracellular uptake of ICG@HMSNPs was better compared to free ICG, and that the fluorescence of ICG was turned on inside the cells. The brighter fluorescence (2.75 times higher than that of free ICG) observed is attributed to the release of ~44% of ICG from the nanoparticles after 4 h incubation. The authors also observed an increased cytotoxicity of ICG@HMSNPs compared to free ICG, which is attributed to a higher intracellular uptake of ICG@HMSNPs. The photodynamic therapeutic effect is also much higher with ICG@HMSNP than free ICG when irradiated at 810 nm (1 W cm^{-2} for 10 mn). This is also due to the fact that HMSNPs release ICG slowly and continuously once the nanoparticles have been taken up by cancer cells. Moreover, this slow release process is advantageous to improve the circulation time and bioavailability.

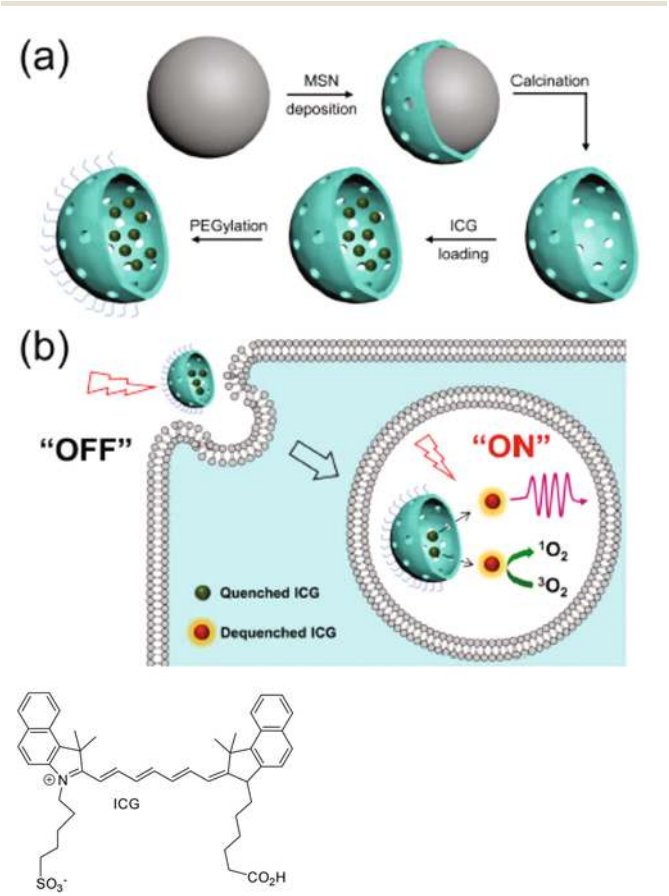

Fig. 15 Scheme of activable near-infrared (NIR) fluorescence imaging and photodynamic therapy using ICG loaded HMSNPs. (a) Synthesis of ICG-loaded HMSNPs (ICG@HMSNP). (b) Fluorescence emission and singlet oxygen ($^1O_2$) generation of ICG were quenched in HMSNPs (aggregation of ICG in HMSNPs). After endocytosis into cancer cells, ICG is released from the HMSNPs, after which ICG becomes highly fluorescent and phototoxic. Reproduced with permission from ref. 71, Copyright 2017 IOPscience.

The expansion of antibiotic resistance leads to the necessity of exploring new anti-bacterial methods. Photodynamic inactivation (PDI) is an alternative treatment method of paramount importance in the post-antibiotic era. PDI efficiency is usually better against Gram-positive bacteria than Gram-negative bacteria. Silver nanoparticles (SNPs) are the most active agents against Gram-negative bacteria, including *Escherichia coli* (*E. coli*), and many others. Therefore, Kuthati *et al.* synthesized curcumin (cur) loaded in copper-impregnated mesoporous silica nanoparticles (Cu-MSN) decorated with SNPs through $NHNH_2$ coordination, presented in Fig. 16.[72] They treated *E. coli* with Cu-MSNs or Cur-Cu-MSNs with or without SNPs at different concentrations. Cur-Cu-MSN-SNPs showed a good bacterial killing efficacy in a dose-dependent manner upon light activation as a result of a photo-enhanced release of silver ions and curcumin activation. Toxicity in the dark was negligible. The results revealed that the Cur-Cu-MSN-SNP nanohybrid compound has all attributes of a good PDI agent against *E. coli* because of the synergistic influence of silver, Cu and curcumin when compared to sole curcumin and SNP modified Cu-MSNs.

6. Synergistic therapies with MSN based PDT

6.1. PDT-drug delivery

Combining chemo- and phototherapy proved to be an efficient strategy for cancer treatment. Because antibody therapy represents a promising alternative to chemotherapy, the conjugation of photosensitizers (PS) with monoclonal antibodies (mAbs) is of interest. Since mesoporous silica nanoparticles

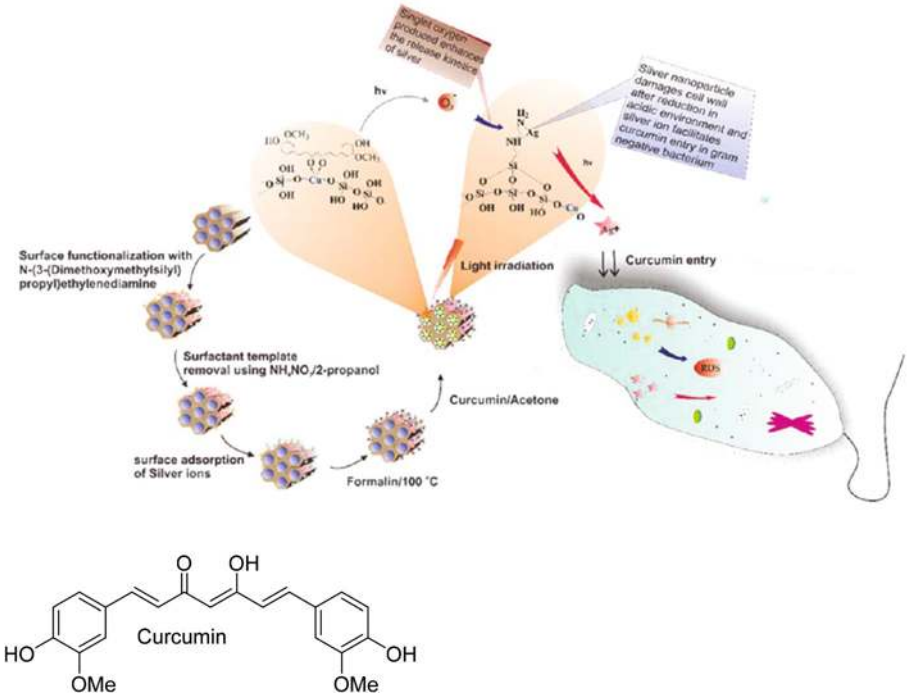

Fig. 16 Schematic illustration of surface modification and plausible mechanism of the antibacterial efficacy of curcumin and SNP immobilized Cu-MSN. Reprinted from ref. 72, with permission from Elsevier.

with small pores are not suitable to incorporate and deliver big biomolecules such as mAbs, Yu and coworkers used dendritic mesoporous silica nanoparticles (DMSNs) with large and open pore channels.[73] Core–shell nanoparticles were synthesized with (i) a solid core doped with fullerene C_{60} acting as a PS for PDT and a dye for imaging (ii) a dendritic shell functionalized with hydrophobic C_{18} chains to load mAbs anti-pAkt (Fig. 17). These core–shell structures are uniform and monodisperse with a mean diameter of 119 nm ± 1 nm (hydrodynamic radius measured by DLS = 121 nm). They present large mesopores with a broad pore size of 28 nm. The BET surface area and pore volume are 294 $m^2\ g^{-1}$ and 1.01 $cm^3\ g^{-1}$, respectively.

The presence of C_{60} was evidenced from the UV-visible and IR spectroscopy data. Generation of $^1O_2$ upon irradiation with UV light is effective according to photobleaching experiments with 9,10-anthracenediylbis(methylene) dimalonic acid. A loading capacity of 12 μg of mAbs anti-pAkt per mg of DMSNs functionnallized with C_{18} was determined. MCF-7 treated with DMSNs show red fluorescence (due to C60) in the cytoplasm indicating the successful cellular uptake (better for C_{18} modified DMSNs compared to the non-modified ones). The synergistic effect of PDT and therapeutic mAb anti-pAkt was investigated. These DMSNs deliver mAbs anti-pAkt more efficiently than if mAbs were used alone (cell viability is 45% with a nanoparticle concentration of 125 μg mL^{-1}, whereas it is 94% with a concentration of mAbs anti-pAkt of 15 μg mL^{-1}). After 5 min irradiation, the cell viablity dropped to 23% showing that PDT and antibody delivery are both effective. Control experiments revealed that the Bcl-2 protein (an antiapoptotic protein) level in MCF-7 decreased upon treatment with DMSNs suggesting an improved delivery of mAbs anti-pAkt compared to the experiment where mAbs are used alone (no DMSNs). Interestingly, UV irradiation caused an additional decrease of Bcl-2 protein level, demonstrating the efficiency of combined antibody/photodynamic therapy for cancer therapy.

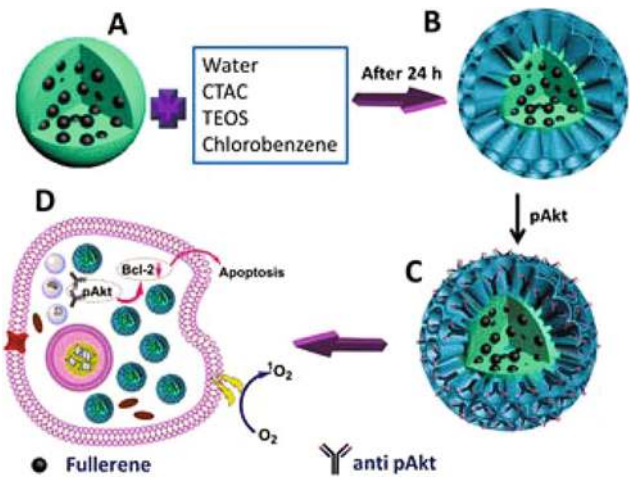

Fig. 17 Schematic illustration of the procedure of FD (core–shell silica–fullerene@DMSN) for applications in imaging and combined protein/PDT. Reproduced with permission from ref. 73, Copyright 2017 Wiley-VCH Verlag GmbH & Co. KGaA, Weinheim.

Tong *et al.* developed NIR-activated (980 nm) theranostic nanocomposites by combining PDT and chemotherapy.[74] They

prepared core $NaYF_4$:Tm,Yb@$NaYF_4$ particles post-coated with mesoporous silica to achieve core–shell nanoparticles (UCNPs@$mSiO_2$). The post modification step was utilized to incorporate TiO_2 (as a photosensitizer) nanoparticles in the pores. This supplies plenty of space to store doxorubicin (DOX) molecules in the pores as well. A UV sensitive *o*-nitrobenzyl derivative gate-keeper (TC) was prepared and grafted after DOX encapsulation to avoid the premature release of DOX. UV emission from the core $NaYF_4$:Tm,Yb@$NaYF_4$ upon NIR irradiation could stimulate TiO_2 to produce singlet oxygen and induce the photodecomposition of TC binder and therefore DOX release (Fig. 18). The HeLa cell viabilities incubated with different concentrations of UCNPs@$mSiO_2$/TiO_2 and DOX-UCNPs@$mSiO_2$/TiO_2-TC were analyzed using the MTT assay. The cell viability did not decrease obviously when the concentration of the sample increased, without irradiation. The combination of PDT and chemotherapy induced enhanced cytotoxicity of DOX-UCNPs@$mSiO_2$/TiO_2-TC to HeLa cells under NIR irradiation. DOX-UCNPs@$mSiO_2$/TiO_2-TC holds promise for the treatment of cancer by NIR light with minimum side effects.

Another approach has been published by Liu *et al.* on the fabrication of MSN@C-dots/RB that incorporates C-dots and rose bengal (RB) with multiple functionalities for drug delivery, synergistic chemo/photodynamic cancer treatment and bacteria inhibition (Fig. 19).[75] The presence of C-dots in the nanostructures and RB allowed cell fluorescence imaging and efficient PDT. They obtained 1.4 times higher singlet oxygen generation in their multifunctional nanostructure under 10 min light irradiation (540 nm) than RB alone. Additionally, antimicrobial assay showed an important bacterial (*E. coli*) inhibitory effect by loading ampicillin into the MSNs@C-dots/RB nanoparticles.

MSNs@C-dots with and without RB and DOX, under light or not were investigated to treat H1299 cancer cells. The associated therapy showed a crucially enhanced therapy relative to single chemotherapy or PDT. Their outcomes displayed considerably enhanced cancer treatment in the human lung cancer cell line NCI-H1299 (H1299) *in vitro* because of the synergistic chemo/photodynamic therapy impact.

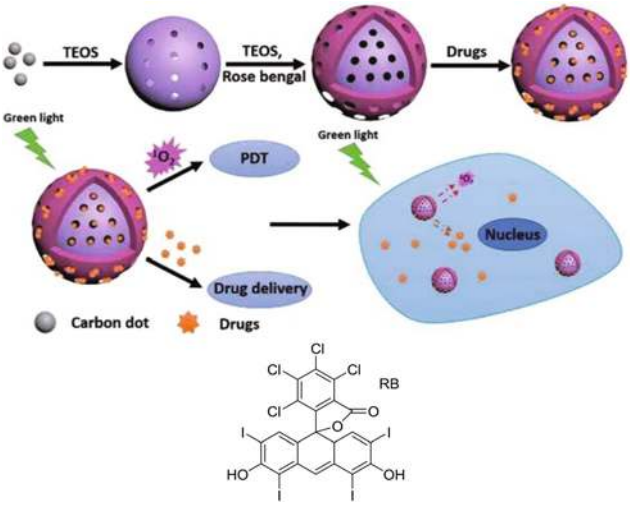

Fig. 19 Illustration of the multifunctional nanoplatform based on MSNs. Reproduced from ref. 75 with permission from the Royal Society of Chemistry.

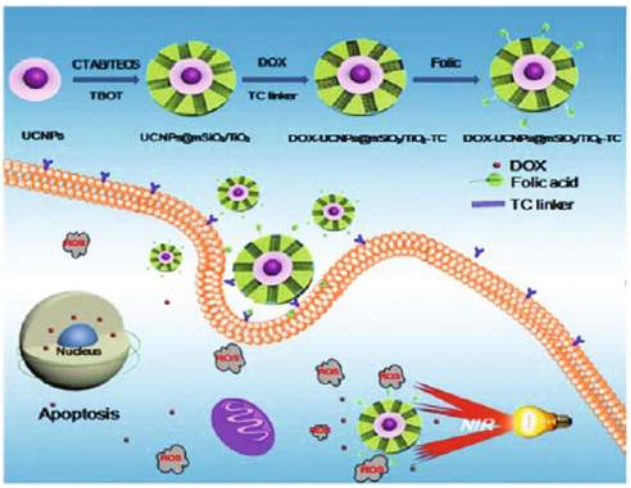

Fig. 18 Illustration of the synthesis and chemo/photothermal synergistic therapy under single 980 nm NIR light. Reprinted from ref. 74, with permission from Elsevier.

Supramolecular PSs (supraPSs) are attracting much attention as efficient photodynamic therapy (PDT) agents owing to their superior photodynamic characteristics. These supramolecular compounds efficiently produce singlet oxygen even at high concentrations. Chen and collaborators used a supraPSs assisted assembly method to easily construct a multiple theranostic nanostructure for tumor-targeted treatment.[76] The multiple nanoplatform (TPZ@MCMSN) was achieved by coating tirapazamine (TPZ)-loaded MSNs using a layer-by-layer (LbL) assembled multilayer. The multilayer was composed of cyclodextrin-conjugated hyaluronic acid, and tetraphenylporphyrin sulfonate (TPPS) was included in the cyclodextrin moiety by host–guest interactions. The porphyrin moiety was metallated with paramagnetic Gd^{3+} ions. The TPZ@MCMSN-Gd^{3+} could be particularly taken up by the CD44 receptor overexpressed in tumor cells and reacted with hyaluronidase (HAase) to activate the release of TPZ (Fig. 20).

The cell viability of COS7, MCF-7, and SCC-7 was assessed *via* MTT assay under various pO_2 conditions. SupraPS based PDT with TPZ demonstrated superior advantages over single therapy, which removes tumor cells synergistically, in the hypoxic medium with limited PDT. The *in vivo* tumor-targeting capacity of TPZ@MCMSN-Gd^{3+} was examined on SCC-7 tumor-bearing nude mice *via* NIR fluorescence and MR imaging. Both the NIR and MR results strictly demonstrated the preferable tumor accumulation of TPZ@MCMSN-Gd^{3+}. TPZ@MCMSN-Gd^{3+} has potential advantages such as efficient tumor targeting, enzyme (HAase)-responsive drug release, dual-modal imaging, and inhibition of the tumor progression

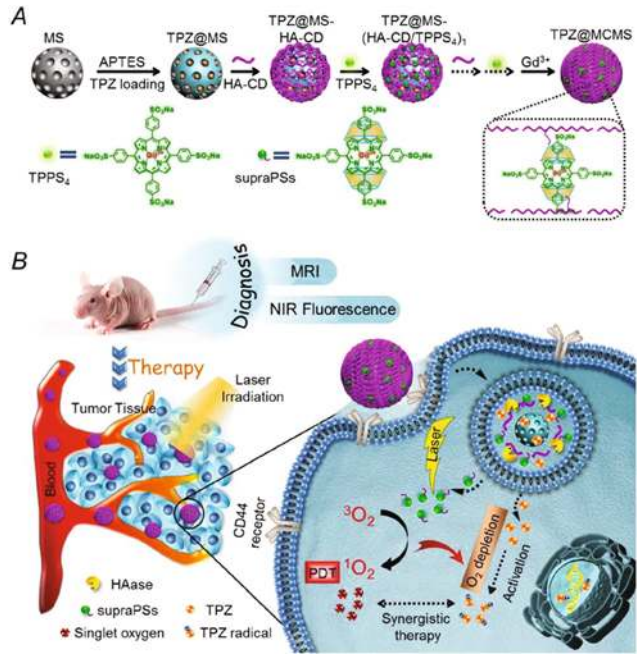

Fig. 20 (A) Layer-by-layer assembly of HA-CD and TPPS4 on TPZ loaded MSNs to prepare the theranostic nanoplatform TPZ@MCMSN-Gd^{3+}. (B) Schematic illustration of the tumor-targeted versatile theranostic nanoplatform to achieve a superior antitumor efficacy by the cooperation of supraPSs-based PDT and bioreductive chemotherapy. Reprinted from ref. 76, with permission from Elsevier.

via the association of PDT and bioreductive chemotherapy upon NIR fluorescence/MR imaging. The combination of supraPSs and a bioreductive prodrug offers an alternative perception to deal with malignant tumors.

Wong *et al.* studied an original mesoporous silica nanoparticle that contains a zinc(II) phthalocyanine (ZnPc)-based photosensitizer attached to DOX *via* an acid-cleavable hydrazone binder (Fig. 21).[77] The high uptake of ZnPc by human hepatocellular carcinoma HepG2 cells was evidenced through the strong intracellular fluorescence intensity. The hydrazone binder was cleaved inside the acidic subcellular divisions of the cells as a result of the co-appearance of ZnPc with DOX fluorescence.

The cytotoxicity of the nanosystems against HepG2 cells was investigated without and with light irradiation (Fig. 22). By regulating the dose of light, the photocytotoxicity of immobilized ZnPc along with the chemocytotoxic DOX effect functioned synergistically. Combination index (CI) values were measured for the cytotoxicities of the drugs detected *via* the MTT assay to study the association mode of PDT and chemotherapy. As seen in Table 1, when the ZnPc concentration was 4 μM ([DOX] = 1.26 μM), the CI was only 0.27, which proved the synergism of two cytotoxic effects. These nanoparticles have the capacity to operate as a dual therapeutic agent with the combination of PDT and controlled chemotherapy, and as a nanosystem for pH-controlled drug release.

Photochemical internalization (PCI), derived from the development of PDT, contributes to the endosomal escape of therapeutic drugs with high temporal and spatial control through an external laser. Liu *et al.* described a complex nanosystem based on a core–shell MSN@tLB (LB lipid bilayers) nanocompound for PCI-mediated PDT and chemotherapy on cancer cells.[78] MSNs were encapsulated with the model drug zoledronic acid (ZOL), or the fluorescent dye calcein, then a lipid bilayer was attached onto the MSN surface through a hyperbranched polyethylenimine (PEI) linker, and the lipophilic photosensitizer IR-780 iodide was incorporated into the lipid bilayer (Fig. 23).

The cytotoxicity of the nanoparticles was investigated on MCF-7 cells using the CCK-8 assay. Unloaded nanoparticles had good cytocompatibility. PCI of calcein was monitored by CLSM and was very efficient; after PDT, the dye diffused from the endo/lysosomes to the cytosol of the cells. The therapeutic efficiency of ZOL, MSN-ZOL, and MSN-ZOL@tLB-IR780 was studied on MCF-7 cells without and with NIR laser irradiation (Fig. 24). In the dark, the cells treated with MSN-ZOL@tLB-IR780 exhibited minor cytotoxicity. To highlight the cell apoptosis state, cell nuclei were stained with Hoechst 33342 (blue fluorescence) and PI (red fluorescence) at the same time and visualized by confocal laser scanning microscopy (CLSM). The MSN-ZOL@tLB-IR780 group at 808 nm demonstrated higher apoptosis than ZOL and MSN-ZOL groups. The MSN-PEI-ZOL@tLB-IR780 nanoplatform displayed high stability, high biocompatibility, and also no significant dark toxicity properties. Under 808 nm laser irradiation, it can produce singlet oxygen to damage endo/lysosomal membranes for the release of the PCI-mediated cytotoxic agent (ZOL) from MSNs into the cytoplasm, hence yielding associated chemotherapy-PDT against cancer cells.

Light-responsive drug delivery systems can release drug into a tumor at the desired time in a controlled manner. Shiqiang and coworkers[79] reported the synthesis of light responsive cyclodextrin (CD) containing chlorin e6 (Ce6) as a photosensitizer for PDT (Fig. 25). MSNs used were MCM-41 type with a mean diameter of ~100 nm, a surface area of 1077 $m^2\ g^{-1}$ and a pore size of 2.7 nm. After functionalization of MSNs with APTES, a part of surface amine groups were functionalized with a molecule containing a carboxylic group at one end (to form the covalent amide bonds with the MSNs) and an azo group at the other (enable a host–guest supramolecular interaction with CD). The spacer used contained a $^1O_2$ sensitive bis-(alkylthio)alkene linkage which can be oxidized and cleaved. The remaining free amine groups were functionalized with Ce6 through the formation of amide bonds too. The obtained particles are able to generate $^1O_2$ upon irradiation at 660 nm (0.5 W cm^{-2}). MSNs were loaded with molecular compounds such as rhodamine B (RhB, ~50 μmol per gram of MSNs) and CDs interacting with the azo groups were used as a gatekeeper. Drug release experiments in water showed that RhB can be released upon irradiation with red light. The release can be well controlled with a 660 nm laser, because the $^1O_2$ produced by Ce6 can further cleave the linker to trigger the departure of CD. Switching experiment results showed that the release was stopped when the laser was switched off confirming that there

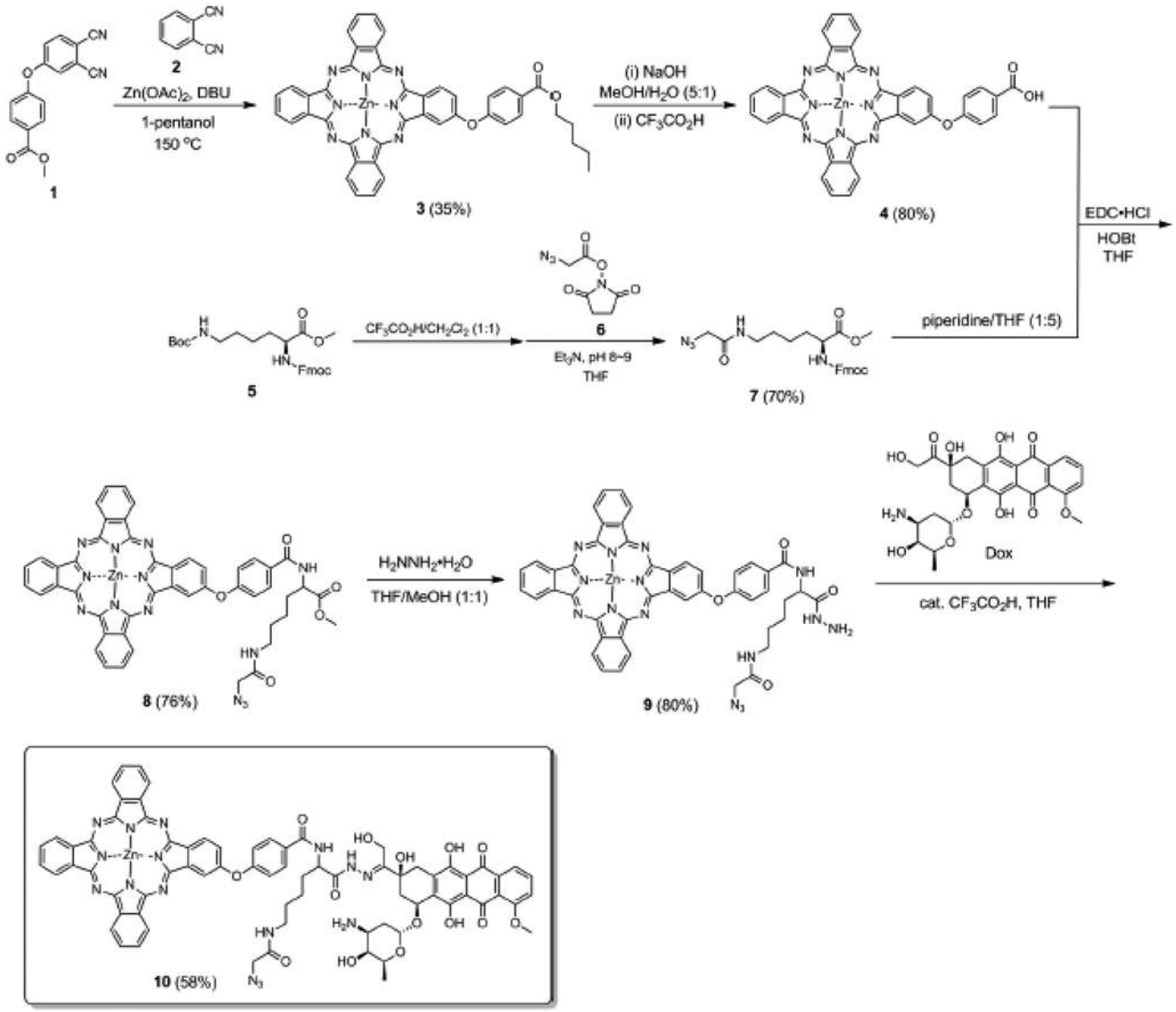

Fig. 21 Synthesis of ZnPc–Dox conjugate 10. Reproduced with permission from ref. 77, Copyright 2017 Wiley-VCH Verlag GmbH & Co. KGaA, Weinheim.

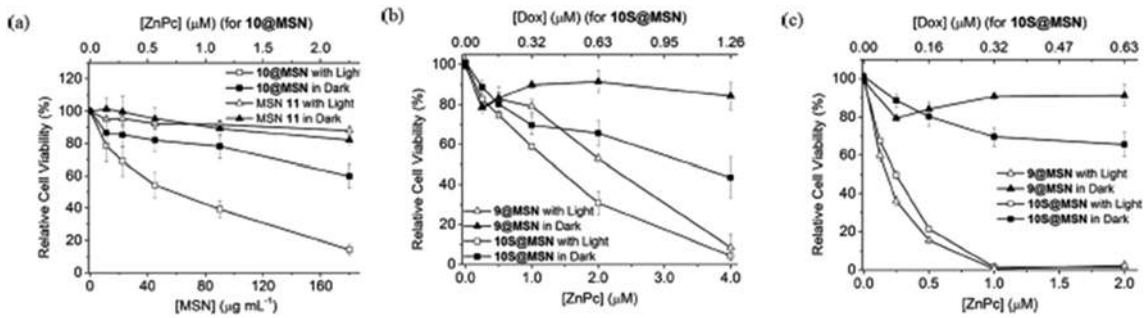

Fig. 22 Cytotoxic effect of MSN 11 and 10@MSN (a), and 9@MSN and 10S@MSN (b) in the absence or presence of light irradiation (λ > 610 nm, 40 mW cm^{-2}) for 20 min. (c) Cytotoxic effect of 9@MSN and 10S@MSN in the absence or presence of light irradiation (λ > 610 nm, 40 mW cm^{-2}) for 1 min. Reproduced with permission from ref. 75, Copyright 2017 Wiley-VCH Verlag GmbH & Co. KGaA, Weinheim.

Table 1 Combination index (CI) based on MTT results at different concentrations of ZnPc and DOX at a fixed ratio (1 : 0.31) in 10S@MSN

Concentration of ZnPc (μM)	Concentration of DOX (μM)	CI
4	1.26	0.27
2	0.63	1.01
1	0.31	1.46
0.5	0.16	1.49
0.25	0.08	1.17

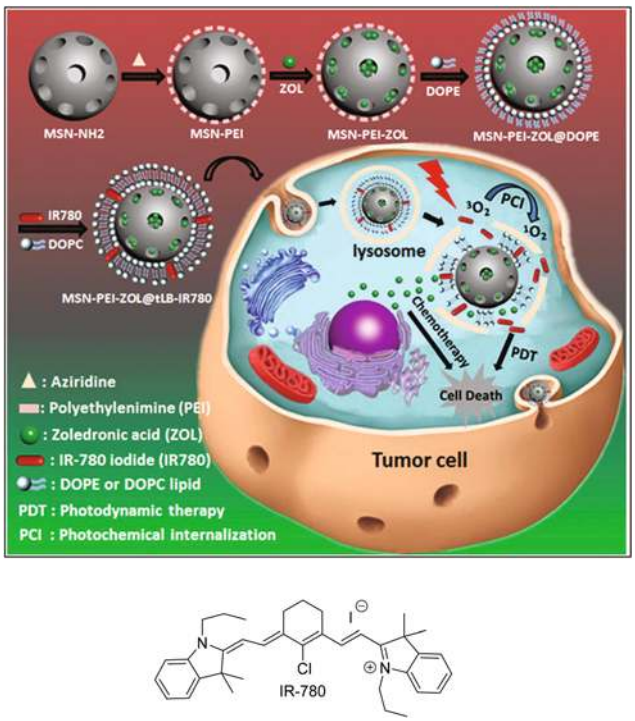

Fig. 23 Schematic representation of the preparation of ZOL and the IR-780 co-loaded MSN@tLB-based drug delivery system and the mechanism of endosomal escape and drug release for combination of PDT and chemotherapy. Reproduced from ref. 78 with permission from the Royal Society of Chemistry.

is no outward diffusion of RhB. *In vitro* experiments on HeLa cells were performed with calcein (a green fluorophore, which can be excited at 488 nm) as model cargo. CDs functionalized with folic acid (FA) target ligand were used as a gatekeeper, since FA receptors are over-expressed by various cell lines such as HeLa cells. *In situ* drug release experiments at the cellular level were performed with MSN-linker-azo/Ce6@calcein@CD-FA nanoparticles. Before irradiation, red and green fluorescence of Ce6 and calcein were perfectly colocalized within the cell, indicating that the MSNs were internalized and that calcein was trapped inside the nanoparticles. After irradiation at 660 nm (0.5 W cm^{-2}), the green fluorescence quickly (1–3 min) spread out into the entire cell due to the release of calcein in the cytosol. Indeed, these MSNs are suitable for the light triggered release of drugs with spatio-temporal controllability. Moreover, PDT is also efficient

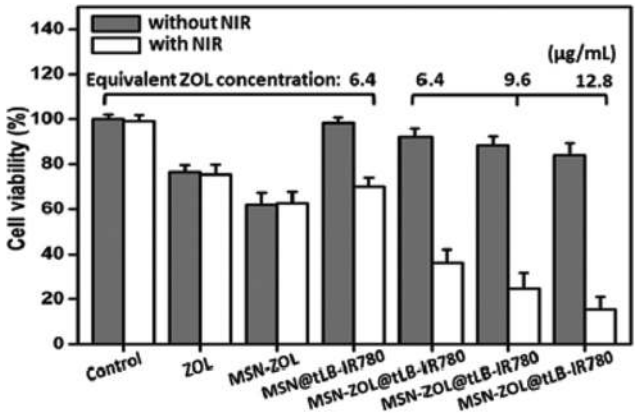

Fig. 24 *In vitro* cell evaluation of the cancer cell inhibition effect. Cell viability of MCF-7 cells after different treatments with or without NIR irradiation (808 nm, 1.2 W cm^{-2}, 10 min). Reproduced from ref. 76 with permission from the Royal Society of Chemistry.

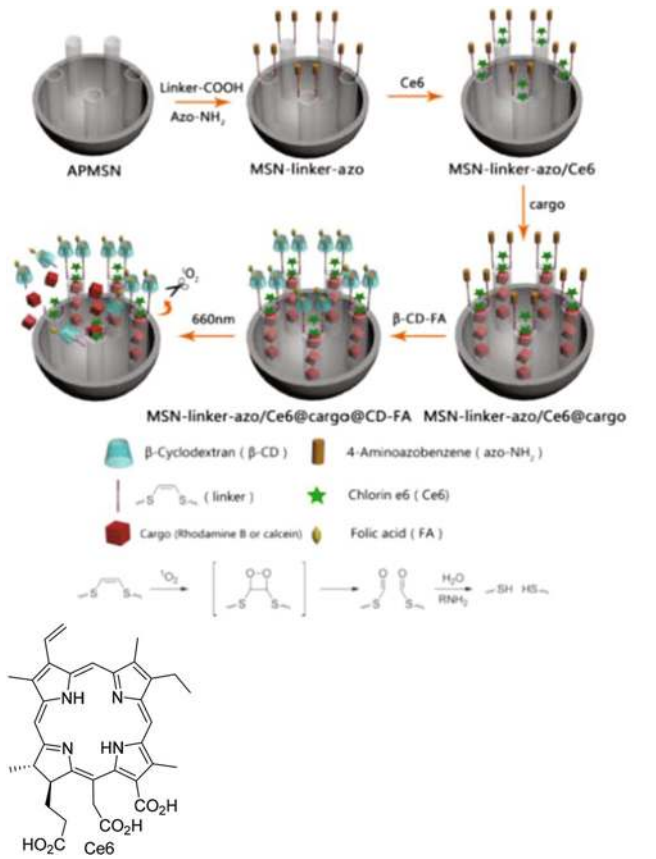

Fig. 25 Synthesis of CD-FA-gated MSNs functionalized with linker-azo and Ce6 and the release of cargo encapsulated in the pores of MSNs. The mechanism of bond cleavage by singlet oxygen is given. Reproduced with permission from ref. 79, Copyright 2017 IOPscience.

because the viability of the cells was significantly decreased upon irradiation (~80% cell death).

An interesting strategy was proposed to achieve maximal chemotherapeutic efficacy of doxorubicin (DOX) and improve

the photodynamic efficiency of rose bengal (RB) through their encapsulation in MSNs.[80] Fig. 26 summarizes the different steps used to construct the pH-sensitive RB and DOX loaded mesoporous silica nanoparticle (MSNs-AH-DOX@RB) nanosystem. The MSNs were functionalized with a pH-sensitive linker, 4-hydrazinobenzoic acid (HBA). RB was then loaded into the HBA-functionalized MSNs, followed by DOX immobilization to the linker through hydrazone bond formation to yield the MSN-AH-DOX@RB nanoplatform.

The *in vitro* release of RB and DOX from MSN-AH-DOX@RB was determined by dialysis in PBS at pH 7.4 and 5.5 at 37 °C. The absence of DOX release at pH 7.4 indicates that the nanoplatform displays a good stability under physiological conditions. A completely different behavior was observed at pH 5.5, where a significant DOX release was obtained. Meanwhile the release of RB remained very limited at both pH values.

The ability of MSN-AH-DOX@RB for $^1O_2$ production under 532 nm laser irradiation (0.5 W cm^{-2}) was evaluated. It was found that the amount of $^1O_2$ generated under these conditions was quite low. This has been ascribed to the strong absorption of light by the external DOX layer. Indeed, upon DOX release under acidic conditions, the nanoplatform can generate $^1O_2$ efficiently.

The *in vitro* cellular toxicity of free DOX, free RB, MSN-AH@RB, MSN-AH-DOX, and MSN-AH-DOX@RB on MCF-7 cells was analysed using the CCK-8 assay. In the dark, all these systems exhibited low cytotoxicity. Upon laser irradiation for 5 min, MSN-AH-DOX@RB displayed the highest cell mortality, suggesting a synergy of chemo-photodynamic treatment.

Another example of multi-functional nanoparticles was reported by Yang *et al.*[81] This system consists of magnetic MSNs loaded with Ce6 and doxorubicin (DOX), which was additionally coated with biocompatible alginate/chitosan polyelectrolyte multilayers to adsorb P-gp shRNA and achieve pH-responsive drug delivery. This nanoplatform enables several functions such as MR and CT imaging, and combined PDT and chemotherapy. The P-gp shRNA was used to reverse the multidrug resistance. The different steps for the synthesis of the nanosystem (M-MSN(Dox/Ce6)/PEM) are summarized in Fig. 27.

Briefly, M-MSNs were prepared by a sol–gel method and subsequently functionalized with APTS to produce amine-terminated nanoparticles (M-MSNs-NH_2). Simple mixing of DOX, Ce6 and M-MSNs-NH_2 was performed to load DOX and Ce6 on the nanoparticles (M-MSN-DOX/Ce6). The M-MSN(DOX/Ce6)/PEM/P-gp shRNA nanocomposite was obtained through functionalization of M-MSN-DOX/Ce6 with biocompatible ALG/CHI polyelectrolyte multilayers (PEM), followed by electrostatic adsorption of P-gp shRNA.

In vitro drug release profiles of DOX and Ce6 from M-MSN (DOX/Ce6)/PEM were studied at two different pH values, namely 7.4 and 4.0, at 37 °C. The results revealed that DOX and Ce6 release from the nanoplatform was pH-dependent with a high release at low pH (4.0). For example, only 12% of Ce6 were released at pH 7.4 over 30 h, while almost complete

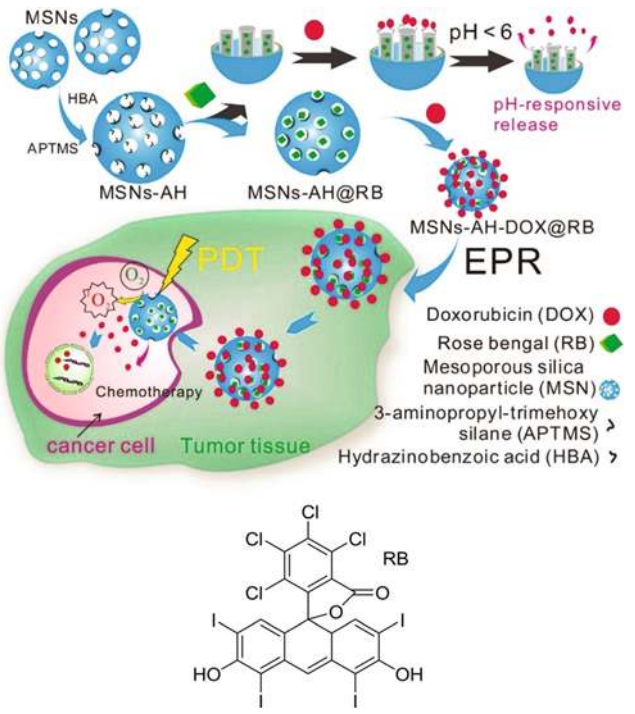

Fig. 26 Schematic illustration of the synthesis of the pH-sensitive MSNs-AH-DOX@RB for controlled drug release. Reprinted from ref. 80, with permission from Elsevier.

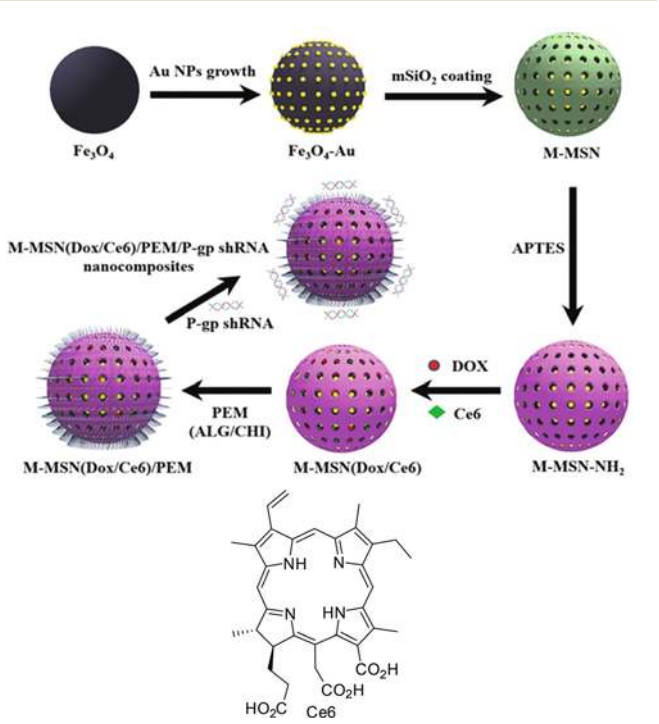

Fig. 27 Procedure for the synthesis of M-MSN(DOX/Ce6)/PEM. Reproduced from ref. 81 with permission from the Royal Society of Chemistry.

release (>95%) was achieved at pH 4.0 over 36 h. A similar trend was observed for DOX release with a less marked contrast. Indeed, 30% release was obtained at pH 7.4 over 32 h; this value increased to 46% at pH 4.0 after 32 h.

The cytocompatibility of M-MSN/PEM nanoparticles was demonstrated on MCF-7, EMT-6 and HUVEC cell lines using the CCK-8 assay. The nanoparticles exhibited no obvious cytotoxicity for all investigated concentrations (20, 50, 100 and 200 μg mL^{-1}) after 24 or 48 h incubation. Similarly, the M-MSN/PEM nanoparticles were homocompatible with limited hemolysis (~5%) activity of the human red blood cells detected for a wide concentration range (25–400 μg mL^{-1}).

The efficacy of the M-MSN(DOX/Ce6)/PEM/P-gp shRNA nanocomposite for cancer cell killing *in vitro* was assessed on various cell lines, including MCF-7, EMT-6 and MCF-7/ADR cells under laser irradiation (660 nm). The results showed a great decrease of cell viability even for drug-resistant tumour cells (MCF-7/ADR) with more than 60% inhibition. The data also clearly indicated that the combined therapy was much more efficient than any monotherapy performed under these experimental conditions. The mechanism of inhibition of cell proliferation induced by M-MSN(DOX/Ce6)/PEM/P-gp shRNA upon laser irradiation was ascribed partially to an apoptotic effect.

In vivo studies performed on EMT-6 tumor-bearing Balb/c mice confirmed that the combined chemotherapy, PDT and gene therapy was very efficient to remove/eradicate the tumour in mice without apparent body weight loss, suggesting that the treatment with M-MSN(DOX/Ce6)/PEM/P-gp shRNA + laser was not toxic to the mice. The results were further corroborated by histological analysis showing limited adverse effects of the main organs.

Finally, the potential of M-MSN(DOX/Ce6)/PEM/P-gp shRNA as a nanoprobe for CT/MR dual-modal imaging and MR imaging of tumours was demonstrated *in vitro* and *in vivo*, respectively.

Liu and coworkers reported the synthesis of core–interlayer–shell Fe_3O_4@$mSiO_2$@lipid-PEG-methotrexate nanoparticles (FMLM) for multimodal imaging and chemo-photodynamic therapy.[82] Fe_3O_4 nanoparticles were prepared by coprecipitation of Fe^{2+} and Fe^{3+} upon addition of NH_3 aq. Then, a mesoporous silica ($mSiO_2$) interlayer was added according to a modified Stöber procedure to obtain the corresponding FM nanoparticles. The cores contain one or more Fe_3O_4 nanocrystals. The shell is mesoporous: the BET surface area of FM nanoparticles is 516.66 m^2 g^{-1}, with a cumulative pore volume of 0.5 cm^3 g^{-1} and an average pore size of 3.89 nm. Finally, the obtained FM nanoparticles were covered with methotrexate (MTX) conjugated PEGylated liposomes (Fig. 28).

Doxorubicin (DOX) and zinc phthalocyanine (ZnPc) were used as a chemotherapeutic and photosensitizer for PDT, respectively. Their encapsulation was performed at different stages of the synthesis of FMLM. The chemotherapeutic agent DOX was encapsulated in the $mSiO_2$ interlayer by treating FM with DOX overnight. ZnPc was encapsulated into the bilayer membrane of liposomes. The obtained FMLM have a mean diameter of ~230 nm and their surface is negatively charged (zeta potential ~−22.6 mV), providing electrostatic stability at physiological pH. The external shell consisting of methotrexate conjugated PEGylated liposomes brings several advantages: (i) it acts as a stopper preventing premature release of DOX, (ii) it allows the hydrophobic ZnPc to be incorporated in the shell, (iii) their methotrexate groups act as tumor targeting ligands for folic acid (FA) receptors, (iv) it extends the circulation time, suppresses macrophage uptake and retards *in vivo* clearence. FMLM nanoparticles conjugated with MTX, which is a FA analogue, are more internalized in FA receptor-positive

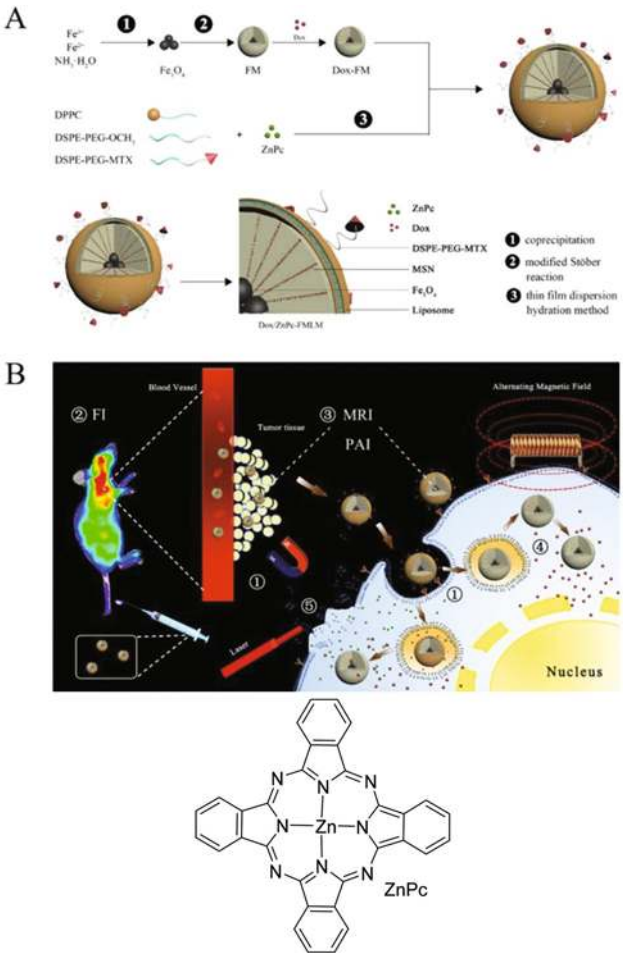

Fig. 28 (A) Schematic routes for the synthesis and drug loading of FMLM. (B) Schematic illustrations of the FMLM on multimodal theranostic and synergistic PDT–chemo-cancer therapy. (1. Multistage targeting strategy of FMLM depends on early-phase magnet targeting cooperated with late-phase active cellular targeting by folate receptor-mediated endocytosis; 2. DOX/ZnPc-FMLM used as a self-fluorescent tracker by ZnPc in fluorescence imaging; 3. FMLM used as both a MRI contrast agent and PAI agent in the multimodal diagnosis platform; 4. the encapsulated DOX was released in the acidic tumor environment in a pH-responsive and magnet-stimulated response manner, magnetic vibration resulted in increasing DOX release with the help of AMF; 5. PDT of DOX/ZnPc-FMLM irradiated by 630 nm laser irradiation.) Reprinted from ref. 82, with permission from Elsevier.

HeLa cells compared to FML nanoparticles without MTX. This is not the case with FA receptor-negative A549 cells. This active FA receptor-mediated endocytosis results in much stronger antitumor activity for DOX-FMLM nanoparticles conjugated with MTX than for DOX-FMFL nanoparticles without MTX. Again, this is not the case with FA receptor-negative A549 cells. Drug release experiments from DOX-FM and DOX-FMLM nanoparticles showed that the DOX-FMLM is quite stable at pH 7.4, and that the release for both types of nanoparticles is faster at pH 5.0 than pH 7.4. Application of an alternating magnetic field (AMF) enhanced DOX release and the subsequent cytotoxicity of DOX-FMLM nanoparticles on HeLa cells. DOX-FMLM nanoparticles are also able to generate $^1O_2$ upon irradiation at 431 nm; an *in vitro* experiment on HeLa cells confirmed the formation of ROS within the cells. Indeed, the FLFM nanoparticles co-loading DOX and ZnPc are suitable for chemo-photodynamic therapy and have the potential for multimodal diagnosis by fluorescence imaging (FI), magnetic resonance imaging (MRI), and photoacoustic imaging (PAI). *In vivo* experiments on HeLa tumor bearing mice revealed that the size of the tumors of mice treated with DOX/ZnPc-FMLM nanoparticles was decreased by 9.5-fold compared to the control group without apparent side effects. The treated tumors presented decreased cellularity and increased necrosis demonstrating the great therapeutic effect of DOX/ZnPc-FMLM nanoparticles.

6.2. MSNs PDT combined with photothermal therapy (PTT)

A remarkable study was reported by Jang *et al.*, in which they utilized graphene oxide (GO) coated SiO_2/TiO_2 hollow nanoparticles (GO-HNP) as a nanocarrier (50 nm diameter) of protoporphyrin IX (PpIX), Fig. 29.[83] GO-HNP-PpIX is evaluated for the synergistic efficiency of PDT–PTT on MCF-7 human breast cancer cells *in vitro*. PpIX release was activated through NIR irradiation at 808 nm and LED light was selected rather than a common laser as a reference PDT light source to kill the cancer cells.

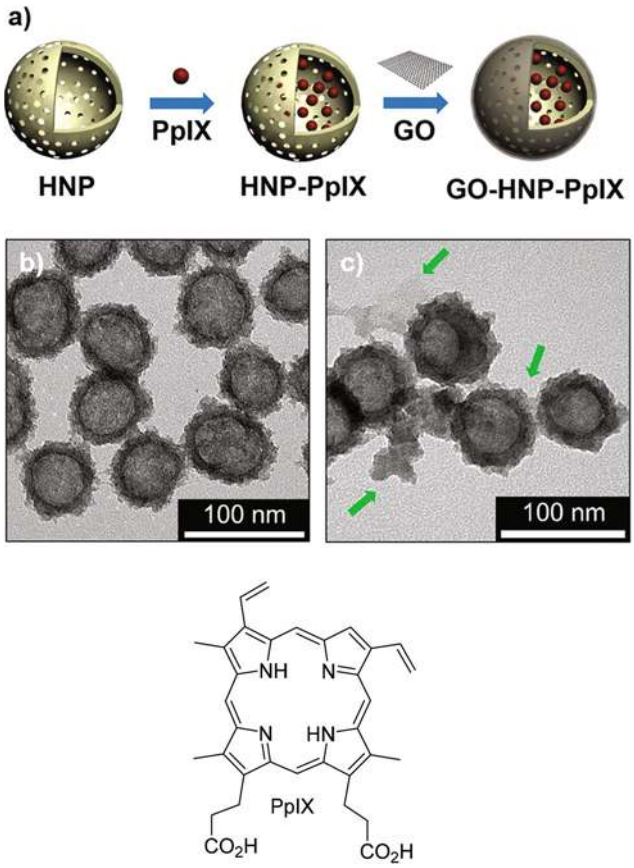

Fig. 29 (a) Schematic representation of the preparation of GO-HNP-PpIX. TEM images of (b) HNP and (c) GO-HNP. (Green arrow shows GO enwrapping of HNPs.) Reproduced with permission from ref. 83, Copyright 2017 Wiley-VCH Verlag GmbH & Co. KGaA, Weinheim.

HNP-PpIX and GO-HNP-PpIX demonstrated very mild dark toxicity toward MCF-7 cells without NIR or Vis-light at different concentrations. The cell killing effect of GO-HNP-PpIX treated MCF-7 cells reached 97.5%, under both NIR light and visible light irradiation which was very efficient. The synergy between NIR irradiation (PTT, PpIX release) and visible light (PDT) was demonstrated. The GO-HNPPpIX/NIR laser/visible-light nanoplatform represents thus an effective external stimuli-responsive anticancer therapy for human breast cancer cells.

Mesoporous silica nanorods (MSNRs) are better than mesoporous silica nanoparticles (MSNPs) in terms of enhanced ability for cell internalization, and higher drug loading performance. The rod-like multi-functional mesoporous silica nanomaterials are important for cell trafficking, cancer cell metastasis monitoring, and drug/DNA delivery. The association of PDT and PTT overcomes the limitations of PDT such as high oxygen dependence. As a PTT agent, Au nanoparticles have superior properties applied to the control of cancer. Sun *et al.* reported MSNRs covalently doped with the Ce6 photosensitizer and capped with gold nanorods (AuNRs), by electrostatic interactions denoted as AuNRs-Ce6-MSNRs, to perform single wavelength light excited PTT/PDT therapy.[84] Ce6 was quenched by the presence of AuNRs. Upon single wavelength NIR irradiation, the PTT effect was obtained which also led to uncapping of MSNRs and activation of Ce6 for PDT. The mechanism of combined PTT/PDT is illustrated in Fig. 30.

Futhermore dual imaging modalities were carried out. Photoacoustic imaging arising from AuNRs and luminescence arising from Ce6 were performed *in vivo*. *In vivo* experiments on 4T1 bearing mice treated with PBS, AuNRs, free Ce6, Ce6-MSNRs and AuNRs-Ce6-MSNRs showed, after 16 days of observation, the smallest tumour volume and weight change for the specimen treated with AuNRs-Ce6-MSNRs. Also, the survival rate was much higher (70%) for the AuNRs-Ce6-MSNRs administered mice, compared to 40% recorded for the other formulations. Histopathological studies corroborated the above results, as confirmed by the significant damage of the tumour tissues such as a decrease of the intercellular space and shrinkage of the cell nucleus. In contrast, no difference in the histopathological features was observed in the major organs (heart, liver, spleens, lung, and kidneys) between the

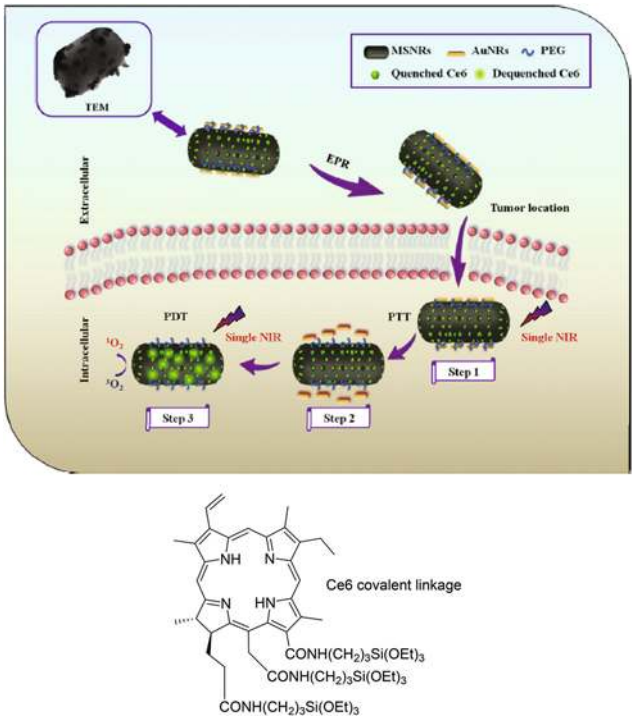

Fig. 30 Illustration of AuNRs-Ce6-MSNRs for synergistic PTT/PDT treatment: (1) under NIR light irradiation, AuNRs generate a localized hyperthermia PTT effect. (2) AuNRs were released from Ce6-doped MSNRs after NIR irradiation. (3) Ce6 was dequenched and then $^1O_2$ was generated, fulfilling the PDT effect. Reprinted from ref. 84, with permission from Elsevier.

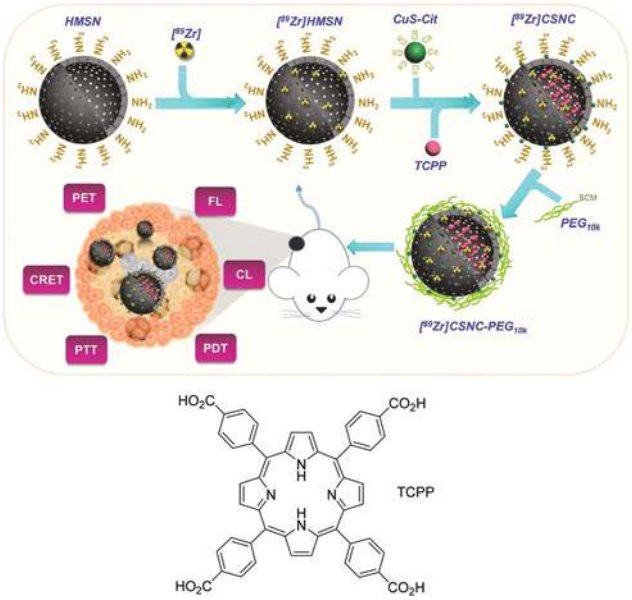

Fig. 31 Schematic illustration of the self-assembly of radiolabeled core–satellite nanoconstructs (CSNC) for simultaneous PET, FL, CL, and CRET imaging and synergistic PTT–PDT in breast-tumor-bearing mice. Reproduced with permission from ref. 85, Copyright 2017 Wiley-VCH Verlag GmbH & Co. KGaA, Weinheim.

control and the AuNRs-Ce6-MSNR treated ones, suggesting that the developed platform represents a suitable candidate for a single wavelength NIR PTT/PDT combined therapy *in vivo*.

Cai and coworkers developed the synthesis of hybrid nanotheranostics integrating organic and inorganic building (nano)blocks for multiple diganostic and therapeutic modalities.[85] These hybrid nanotheranostics are prepared from hollow mesoporous silica nanoparticles (HMSNs) with diameters of ~150 nm radiolabeled with ^{89}Zr ($t_{1/2}$ = 78.4 hours) for dual positron emission tomography (PET) and Cerenkov luminescence (CL) imaging. Meso-tetrakis(4-carboxyphenyl) porphyrin (TCPP) was then encapsulated in HMSNs (Fig. 31).

TCPP can be used as a dye for fluorescence (FL) imaging and, simultaneously, as light harvesting coupled with ^{89}Zr for Cerenkov radiation energy transfer (CRET). TCPP can also be used as a photosensitizer for photodynamic therapy (PDT). The surface of HMSNs was decorated with copper sulfide (CuS) nanoparticles with diameters of ~10 nm and functionalized with citrate, which can be used as a hyperthermia agent for photothermal therapy (PTT) owing to their high photothermal conversion efficiency. There are around 7833 CuS nanoparticles per HMSN firmly bound to their shell, since minimal detachment was observed in high ionic strength physiological solutions at pH 5.5 and 7.4. Indeed, the obtained nanostructures enable tetramodal imaging (PET/FL/CL/CRET) and bimodal therapy (PDT/PTT) for optimal diagnostic and therapy and are stable enough for *in vivo* studies. Finally, the surface core–satellite nanoconstructs (CSNCs) were coated with branched poly(ethylene glycol) to ensure colloidal stability and biocompatibility. The photothermal activity was demonstrated upon irradiation at 980 nm (10 mn, 4 W cm^{-2}) and a rapid transient increase in temperature (T_{max} > 45 °C) was observed. The photodynamic activity was also demonstrated upon irradiation at 660 nm (20 mn, 50 mW cm^{-2}) by quantifying $^1O_2$ generation. *In vivo* experiments were performed on mice bearing subcutaneous 4T1 murine breast tumors and treated with the CSNCs. PET and FL imaging showed prolonged blood circulation and a gradual increase in tumor uptake after 24 h after injection. After intratumoral injection, strong and persistent signals were observed by PET, Cl, CRET and FL. Gradual diffusion of FL signal is in agreement with the release of TCPP molecules from CSNCs. Synergistic photothermal/photodynamic therapy was also investigated, because the interaction between PTT and PDT was found to be more effective than a purely additive one. Such a synergism can be explained by the possible improvement of blood flow in the tumor due to PTT. It increases the oxygenation of the tumor, and this has an important consequence in PDT effectiveness. Excellent results were recorded when combining PTT and PDT, since complete eradication of the tumors was obtained with complete healing 30 days after the treatment.

6.3. PDT–PTT-chemotherapy

Increasing attention is being paid to the design of effective anticancer agents with the combination of versatile imaging

and therapies into a single nanocomposite. Chen and co-workers prepared original core–shell–shell nanoparticles associating PDT, luminescence imaging with photothermal therapy (PTT) and chemotherapy for improved antitumor theranostics. They prepared upconversion (UC) core ($NaYF_4$:Yb, Tm@$NaYF_4$), silica sandwich shell shaped with hypocrellin A (HA)/carbon dots (C-Dots), with mesoporous silica outer-shell (UCNPs@SiO_2-C/HA@mSiO_2) nano-objects.[86] The designed UCNPs@SiO_2-C/HA@mSiO_2 (85 nm in size) nanoplatform was further functionalized with *o*-nitrobenzyl derivative linker (NB linker) as a UV sensitive gate in order to immobilize the anticancer drug (doxorubicin hydrochloride, DOX) inside the mesopores (Fig. 32).

Under 980 nm NIR light irradiation, the UC core emitted UV light, leading to the cleavage of the NB linker and therefore to drug release. The Vis emission at 450–480 nm triggered singlet oxygen generation and PDT by energy transfer to HA while NIR excitation of C-dots led to the PTT effect. Furthermore, UCNPs@SiO_2-C-Dots/HA exhibited green and red luminescence emission in HepG2 cells upon NIR excitation arising from C-Dot and HA doping, respectively. The synergistic cooperation of PTT, PDT and chemotherapy led to very efficient cancer cell killing *in vitro*.

Wang *et al.* synthesized an original core–shell–satellite $NaGdF_4$:Yb,Er,Mn,Co@mSiO_2-CuS nanoplatform containing up-conversion luminescent (UCL) $NaGdF_4$:Yb,Er,Mn,Co as the core, a mesoporous silica shell, photoactive CuS nanoparticles as the satellites, DOX drug and ZnPc photosensitizer, Fig. 33.[87] PDT and chemotherapy properties of the nanoplatform are provided by ZnPc and DOX, respectively. The co-doping of Co^{2+} ions was used for T_2-weighted MRI function, and the co-doping of Gd^{3+} for T_1-weighted MRI and CT imaging. The intrinsic UC luminescence imaging, and the co-doping with Mn^{2+} enhanced the red emission and led to PDT efficiency by excitation of ZnPc *via* the fluorescence resonance energy transfer (FRET) mechanism. Furthermore, the production of heat from the CuS nanoparticles allowed PTT and improved DOX release from the nanosystem under NIR light irradiation.

The viability of L929 fibroblasts was studied using an MTT assay upon incubation with UCNP@mSiO_2-CuS-ZnPc (UMCZ) at different concentrations. The nanoparticles demonstrated high viability up to a concentration of 500 μg mL^{-1}. The tumor-xenografted (liver cancer cell line H22) mice were intratumorally treated through injection of UMCZ in the absence or in the presence of DOX under NIR light or not. When UMCZ-DOX was injected and irradiated with NIR light, the association of heat enhanced chemotherapy and PDT, resulting in the highest tumor inhibition efficacy. A synergistic combination of PDT, PTT and chemotherapy with multiple imaging techniques (MRI, CT, and UCL) demonstrated a significant promising theranostic capacity *in vitro* and *in vivo*.

In another study, Fang *et al.* described a hierarchical nanostructure GNR@mSiO_2-5-FU-ICG – including mesoporous silica-coated gold nanorods as the core, through the coupling of Indocyanine Green (ICG) on the surface, and immobilization of 5-fluorouracil (5-FU) in the mesopores of silica shells – for cancer treatment.[88] ICG was exploited for fluorescence imaging and PDT, and the model drug 5-FU was utilized for chemotherapy. The GNR@SiO_2-5-FU-ICG nanostructure led to

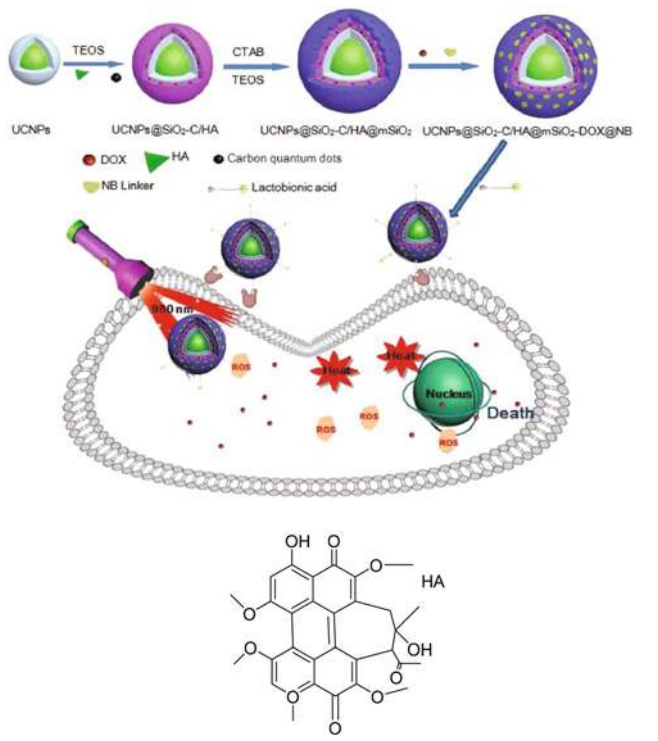

Fig. 32 Schematic illustration of the preparation and multitherapy of a LA-UCNPs@SiO_2-C/HA@mSiO_2-DOX@NB nanocomposite. Reproduced from ref. 86 with permission from the Royal Society of Chemistry.

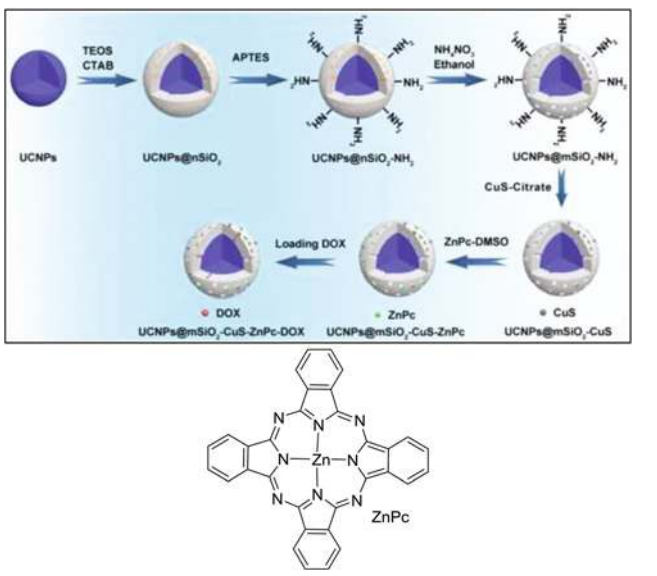

Fig. 33 Schematic presentation of the synthesis of the $NaGdF_4$:Yb,Er, Mn,Co@mSiO_2-CuS-ZnPc-DOX nanocomposite. Reproduced from ref. 87 with permission from the Royal Society of Chemistry.

multiple imaging techniques such as two-photon luminescence, fluorescence, photoacoustic, photothermal imaging, and also trimodal synergistic therapy such as PTT, PDT, and chemotherapy.

The cytotoxicity of GNR@SiO_2-5-FU-ICG was studied on A375 cells using a CCK-8 assay (Fig. 34). GNR@SiO_2-5-FU-ICG displayed better chemotherapeutic effects than free 5-FU, due to the higher cellular uptake efficiency of GNR@SiO_2-5-FU-ICG. The trimodal synergistic therapy of GNR@SiO_2-5-FU-ICG was also examined on A375 cells (laser irradiation at 808 nm). The triple synergism of PTT–PDT-chemotherapy clearly demonstrated superiority over the dual-mode PTT–PDT and also PTT alone. The *in vivo* multimodal imaging guided trimodal synergistic therapy was performed on A375 xenografted-tumor mice. The photoacoustic (PA) signal of mice treated with GNR@SiO_2-5-FU-ICG was much higher in the tumor than that of mice treated with GNR@SiO_2–NH_2, supporting the synergistic effect of GNR@SiO_2 and ICG. The tumor size and weight were measured for the anticancer efficacy of GNR@SiO_2-5-FU-ICG. The efficient killing efficacy of GNR@SiO_2-5-FU-ICG (PTT + PDT + chemotherapy) was proved. The trimodal synergistic therapy-guided multimodal imaging was successful with complete tumor destruction without recurrence.

In a very recent report, Sun *et al.* proposed a NIR-triggered triple modal imaging-guided multi-functional nanoplatform.[89] The nanoplatform consists of doxorubicin (DOX)@Gd-doped MSNs coated with thermosensitive liposomes conjugated with indocyanine green (DOX@GdMSNs-ICG-TSLs). ICG was expected to contribute to both PDT and PTT effects with additional use for NIR fluorescence imaging (NIRFI) as well as photoacoustic imaging (PAI), while Gd allows magnetic resonance imaging (MRI). Coating of DOX@GdMSNs with folic acid-functionalized TSLs was used to improve DOX leakage and cellular uptake. Under NIR light illumination, ICG could generate heat, leading to ICG-TSL rupture and subsequently to DOX release (Fig. 35).

The photothermal properties of PBS, GdMSNs, DOX@GdMSNs, ICG-TSLs, and DOX@GdMSNs-ICG-TSLs nanocomposite were evaluated under 808 nm (1.5 W cm^{-2}) laser irradiation. A temperature increase to 55 °C was observed after 5 min irradiation for both ICG-TSLs and DOX@GdMSNs-ICG-TSLs, while the temperature was below 33 °C for the other components. This clearly highlights the role of ICG in the PTT mechanism. A photothermal conversion efficiency (η) of 11.72% was determined for DOX@GdMSNs-ICG-TSLs. The PDT effect was monitored using DPBF trapping agent upon irradiation at 808 nm for 8 min. Again, the results confirmed that the presence of ICG in the nanoplatform was responsible for $^1O_2$ generation. Similarly, DOX release from DOX@GdMSNs-ICG-TSLs was highly improved under NIR irradiation, indicating the suitability of the platform for combined PTT–PDT-chemotherapy.

Cellular cyctoxicity studies of DOX@GdMSNs-ICG-TSLs with different DOX and ICG concentrations were assessed by MTT assay using PBS, DOX@GdMSNs, ICG-TSLs + NIR as the controls. It was found that the 4T1 cell viabilities decreased by increasing the concentration of DOX or ICG and

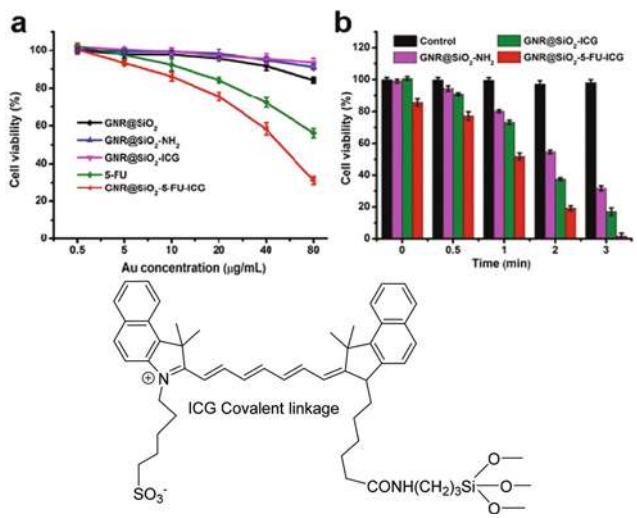

Fig. 34 (a) Cytotoxicity of A375 cells incubated with GNR@SiO_2, GNR@SiO_2–NH_2, GNR@SiO_2-ICG, and 5-FU or GNR@SiO_2-5-FU-ICG at several Au concentrations of 0.5–80 μg mL^{-1}. (b) Cell viability of A375 cells incubated with GNR@SiO_2–NH_2, GNR@SiO_2-ICG, or GNR@SiO_2-5-FU-ICG for 24 h and with laser irradiation (808 nm, 1.5 W cm^{-2}) for different times. Reproduced with permission from ref. 88, Copyright 2017 Wiley-VCH Verlag GmbH & Co. KGaA, Weinheim.

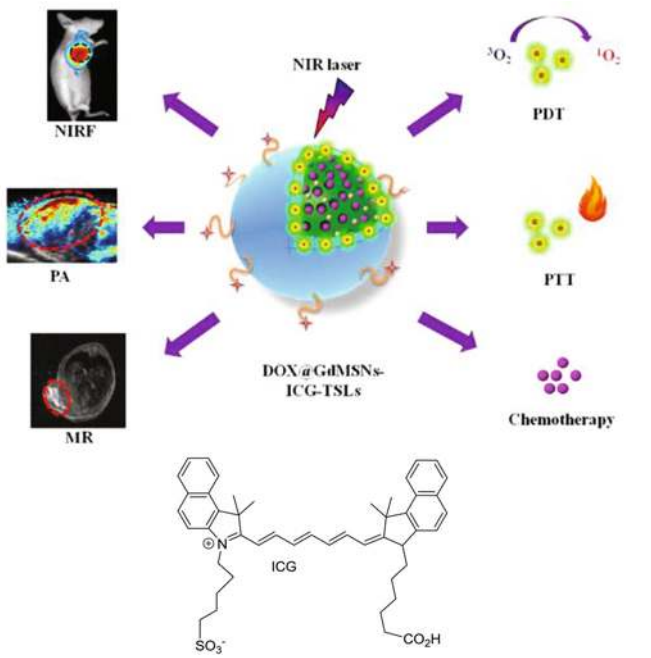

Fig. 35 Schematic presentation of the functions of the DOX@GdMSNs-ICG-TSL theranostic nanocomposite for fluorescence/photoacoustic/magnetic resonance imaging-guided chemo- and phototherapy. Reprinted with permission from ref. 89. Copyright 2018 American Chemical Society.

DOX@GdMSNs-ICG-TSLs + NIR experienced the highest decrease of cell viability, compared to the controls.

In vivo experiments were performed on 4T1 tumour-bearing mice under 808 nm (1.5 W cm^{-2}) laser irradiation of the tumour sites after DOX@GdMSNs-ICG-TSL intravenous injection. The relative tumour volume measured after 20 days was 10.67, 5.03, 5.50, and 1.75 for PBS, DOX@GdMSNs, ICG-TSLs + NIR, and DOX@GdMSNs-ICG-TSLs + NIR, indicating the clear advantages of combined therapy compared to monotherapy. The results are consistent with the slight mice body weight change recorded after DOX@GdMSNs-ICG-TSLs + NIR compared to the controls.

Histological studies confirmed the suitability of the DOX@GdMSNs-ICG-TSLs for tumour treatment, as witnessed by the limited adverse effect on the major organs (heart, liver, spleen, lung, and kidneys), and extensive necrosis and intracellular space decrease in tumour tissue section.

7. Conclusion

Since the pioneering work in 2009 concerning PDT combined with MSNs, the field has expanded and gained in complexity. As shown in this review, very efficient sophisticated MSN-based nanosystems involving PDT have been designed for multimodal imaging (luminescence, PET, MRI, tomography), and targeted controlled multitherapies (PDT, PTT, chemotherapy, radiotherapy). Many systems were prepared based on up-conversion, persistent luminescence, X-ray absorption or sonodynamic therapy for the treatment of deep tumors. Although the majority of the studies described cancer applications, other diseases were also targeted such as Alzheimer's, atherosclerosis or antimicrobial PDT showing the high versatility of MSNs combined with PDT. Therefore, major improvements in PDT have been brought with MSNs. Indeed, a better spatio-temporal control of PDT at the disease site has been demonstrated with MSNs, avoiding general photosensitization usually observed with a classical PS, and multi-therapies with MSNs allow a very efficient treatment of the disease. MSNs have been shown to be biocompatible, but the degradability of MSNs has to be further studied in order to translate MSNs to clinical applications. Therefore MSN based nanosystems combined with PDT could be of great interest for personalized nanomedicine applications in the future.

Conflicts of interest

There are no conflicts to declare.

References

1 H. Huang and J. F. Lovell, Advanced Functional Nanomaterials for Theranostics, *Adv. Funct. Mater.*, 2017, **27**, 1603524.
2 R. R. Castillo, M. Colilla and M. Vallet-Regi, Advances in mesoporous silica-based nanocarriers for co-delivery and combination therapy against cancer, *Expert Opin. Drug Delivery*, 2017, **14**, 229–243.
3 Y. Yang and C. Yu, Advances in silica based nanoparticles for targeted cancer therapy, *Nanomedicine*, 2016, **12**, 317–332.
4 M. van Elk, B. P. Murphy, T. Eufrasio-da-Silva, D. P. O'Reilly, T. Vermonden, W. E. Hennink, G. P. Duffy and E. Ruiz-Hernandez, Nanomedicines for advanced cancer treatments: Transitioning towards responsive systems, *Int. J. Pharm.*, 2016, **515**, 132–164.
5 Y. Feng, N. Panwar, D. J. H. Tng, S. C. Tjin, K. Wang and K.-T. Yong, The application of mesoporous silica nanoparticle family in cancer theranostics, *Coord. Chem. Rev.*, 2016, **319**, 86–109.
6 M. A. Chowdhury, The Controlled Release of Drugs and Bioactive Compounds from Mesoporous Silica Nanoparticles, *Curr. Drug Delivery*, 2016, **13**, 839–856.
7 Y. Wang, Q. Zhao, N. Han, L. Bai, J. Li, J. Liu, E. Che, L. Hu, Q. Zhang, T. Jiang and S. Wang, Mesoporous silica nanoparticles in drug delivery and biomedical applications, *Nanomedicine*, 2015, **11**, 313–327.
8 S. Baek, R. K. Singh, D. Khanal, K. D. Patel, E.-J. Lee, K. W. Leong, W. Chrzanowski and H.-W. Kim, Smart multifunctional drug delivery towards anticancer therapy harmonized in mesoporous nanoparticles, *Nanoscale*, 2015, **7**, 14191–14216.
9 P. N. Dave and L. V. Chopda, A review on application of multifunctional mesoporous nanoparticles in controlled release of drug delivery, *Mater. Sci. Forum*, 2014, **781**, 17–24.
10 K. T. Mody, A. Popat, D. Mahony, A. S. Cavallaro, C. Yu and N. Mitter, Mesoporous silica nanoparticles as antigen carriers and adjuvants for vaccine delivery, *Nanoscale*, 2013, **5**, 5167–5179.
11 V. Mamaeva, C. Sahlgren and M. Linden, Mesoporous silica nanoparticles in medicine-Recent advances, *Adv. Drug Delivery Rev.*, 2013, **65**, 689–702.
12 D. Douroumis, I. Onyesom, M. Maniruzzaman and J. Mitchell, Mesoporous silica nanoparticles in nanotechnology, *Crit. Rev. Biotechnol.*, 2013, **33**, 229–245.
13 F. Tang, L. Li and D. Chen, Mesoporous Silica Nanoparticles: Synthesis, Biocompatibility and Drug Delivery, *Adv. Mater.*, 2012, **24**, 1504–1534.
14 Z. Li, J. C. Barnes, A. Bosoy, J. F. Stoddart and J. I. Zink, Mesoporous silica nanoparticles in biomedical applications, *Chem. Soc. Rev.*, 2012, **41**, 2590–2605.
15 Q. He and J. Shi, Mesoporous silica nanoparticle based nano drug delivery systems: synthesis, controlled drug release and delivery, pharmacokinetics and biocompatibility, *J. Mater. Chem.*, 2011, **21**, 5845–5855.
16 J. L. Vivero-Escoto, I. I. Slowing, B. G. Trewyn and V. S. Y. Lin, Mesoporous Silica Nanoparticles for Intracellular Controlled Drug Delivery, *Small*, 2010, **6**, 1952–1967.

17 I. I. Slowing, J. L. Vivero-Escoto, C.-W. Wu and V. S. Y. Lin, Mesoporous silica nanoparticles as controlled release drug delivery and gene transfection carriers, *Adv. Drug Delivery Rev.*, 2008, **60**, 1278–1288.

18 B. G. Trewyn, I. I. Slowing, S. Giri, H.-T. Chen and V. S. Y. Lin, Synthesis and Functionalization of a Mesoporous Silica Nanoparticle Based on the Sol-Gel Process and Applications in Controlled Release, *Acc. Chem. Res.*, 2007, **40**, 846–853.

19 I. I. Slowing, B. G. Trewyn, S. Giri and V. S. Y. Lin, Mesoporous silica nanoparticles for drug delivery and biosensing applications, *Adv. Funct. Mater.*, 2007, **17**, 1225–1236.

20 E. Yamamoto and K. Kuroda, Colloidal mesoporous silica nanoparticles, *Bull. Chem. Soc. Jpn.*, 2016, **89**, 501–539.

21 N. Z. Knezevic and J.-O. Durand, Large pore mesoporous silica nanomaterials for application in delivery of biomolecules, *Nanoscale*, 2015, **7**, 2199–2209.

22 S.-H. Wu, C.-Y. Mou and H.-P. Lin, Synthesis of mesoporous silica nanoparticles, *Chem. Soc. Rev.*, 2013, **42**, 3862–3875.

23 R. Duan, F. Xia and L. Jiang, Constructing Tunable Nanopores and Their Application in Drug Delivery, *ACS Nano*, 2013, **7**, 8344–8349.

24 Y. Chen, H. Chen and J. Shi, In Vivo Bio-Safety Evaluations and Diagnostic/Therapeutic Applications of Chemically Designed Mesoporous Silica Nanoparticles, *Adv. Mater.*, 2013, **25**, 3144–3176.

25 J. G. Croissant, Y. Fatieiev, A. Almalik and N. M. Khashab, Mesoporous Silica and Organosilica Nanoparticles: Physical Chemistry, Biosafety, Delivery Strategies, and Biomedical Applications, *Adv. Healthcare Mater.*, 2018, **7**, 1700831.

26 Y. Zhang, J. Yan and S. Liu, Biocompatibility and biomedical applications of functionalized mesoporous silica nanoparticles, *Biointerface Res. Appl. Chem.*, 2014, **4**, 767–775.

27 C. Argyo, V. Weiss, C. Braeuchle and T. Bein, Multifunctional Mesoporous Silica Nanoparticles as a Universal Platform for Drug Delivery, *Chem. Mater.*, 2014, **26**, 435–451.

28 L. Pasqua, A. Leggio, D. Sisci, S. Ando and C. Morelli, Mesoporous Silica Nanoparticles in Cancer Therapy: Relevance of the Targeting Function, *Mini-Rev. Med. Chem.*, 2016, **16**, 743–753.

29 J.-J. Hu, D. Xiao and X.-Z. Zhang, Advances in Peptide Functionalization on Mesoporous Silica Nanoparticles for Controlled Drug Release, *Small*, 2016, **12**, 3344–3359.

30 J. Zhu, Y. Niu, Y. Li, Y. Gong, H. Shi, Q. Huo, Y. Liu and Q. Xu, Stimuli-responsive delivery vehicles based on mesoporous silica nanoparticles: recent advances and challenges, *J. Mater. Chem. B*, 2017, **5**, 1339–1352.

31 Y. Chen, H. Zhang, X. Cai, J. Ji, S. He and G. Zhai, Multifunctional mesoporous silica nanocarriers for stimuli-responsive target delivery of anticancer drugs, *RSC Adv.*, 2016, **6**, 92073–92091.

32 R. Sun, W. Wang, Y. Wen and X. Zhang, Recent advance on mesoporous silica nanoparticles-based controlled release system: intelligent switches open up new horizon, *Nanomaterials*, 2015, **5**, 2019–2053.

33 M. Colilla and M. Vallet-Regi, Responsive mesoporous silica nanoparticles for targeted drug delivery, *RSC Smart Mater.*, 2015, **14**, 136–166.

34 A. F. Moreira, D. R. Dias and I. J. Correia, Stimuli-responsive mesoporous silica nanoparticles for cancer therapy: A review, *Microporous Mesoporous Mater.*, 2016, **236**, 141–157.

35 K. K. Coti, M. E. Belowich, M. Liong, M. W. Ambrogio, Y. A. Lau, H. A. Khatib, J. I. Zink, N. M. Khashab and J. F. Stoddart, Mechanised nanoparticles for drug delivery, *Nanoscale*, 2009, **1**, 16–39.

36 Y. Zhao, J. L. Vivero-Escoto, I. I. Slowing, B. C. Trewyn and V. S. Y. Lin, Capped mesoporous silica nanoparticles as stimuli-responsive controlled release systems for intracellular drug/gene delivery, *Expert Opin. Drug Delivery*, 2010, **7**, 1013–1029.

37 B. Ruehle, P. Saint-Cricq and J. I. Zink, Externally Controlled Nanomachines on Mesoporous Silica Nanoparticles for Biomedical Applications, *ChemPhysChem*, 2016, **17**, 1769–1779.

38 Y.-W. Yang, Towards biocompatible nanovalves based on mesoporous silica nanoparticles, *MedChemComm*, 2011, **2**, 1033–1049.

39 J. P. Celli, B. Q. Spring, I. Rizvi, C. L. Evans, K. S. Samkoe, S. Verma, B. W. Pogue and T. Hasan, Imaging and Photodynamic Therapy: Mechanisms, Monitoring, and Optimization, *Chem. Rev.*, 2010, **110**, 2795–2838.

40 C. A. Robertson, D. H. Evans and H. Abraharnse, Photodynamic therapy (PDT): A short review on cellular mechanisms and cancer research applications for PDT, *J. Photochem. Photobiol., B*, 2009, **96**, 1–8.

41 S. S. Lucky, K. C. Soo and Y. Zhang, Nanoparticles in Photodynamic Therapy, *Chem. Rev.*, 2015, **115**, 1990–2042.

42 R. Chouikrat, A. Seve, R. Vanderesse, H. Benachour, M. Barberi-Heyob, S. Richeter, L. Raehm, J. O. Durand, M. Verelst and C. Frochot, Non Polymeric Nanoparticles for Photodynamic Therapy Applications: Recent Developments, *Curr. Med. Chem.*, 2012, **19**, 781–792.

43 F. Figueira, J. A. S. Cavaleiro and J. P. C. Tome, Silica nanoparticles functionalized with porphyrins and analogs for biomedical studies, *J. Porphyrins Phthalocyanines*, 2011, **15**, 517–533.

44 S.-H. Cheng and L.-W. Lo, Inorganic nanoparticles for enhanced photodynamic cancer therapy, *Curr. Drug Discovery Technol.*, 2011, **8**, 250–268.

45 P. Couleaud, V. Morosini, C. Frochot, S. Richeter, L. Raehm and J. O. Durand, Silica-based nanoparticles for photodynamic therapy applications, *Nanoscale*, 2010, **2**, 1083–1095.

46 D. K. Chatterjee, L. S. Fong and Y. Zhang, Nanoparticles in photodynamic therapy: An emerging paradigm, *Adv. Drug Delivery Rev.*, 2008, **60**, 1627–1637.

47 D. Bechet, P. Couleaud, C. Frochot, M.-L. Viriot, F. Guillemin and M. Barberi-Heyob, Nanoparticles as vehicles for delivery of photodynamic therapy agents, *Trends Biotechnol.*, 2008, **26**, 612–621.

48 Y. Zhou, X. Liang and Z. Dai, Porphyrin-loaded nanoparticles for cancer theranostics, *Nanoscale*, 2016, **8**, 12394–12405.

49 Y. Shen, A. J. Shuhendler, D. Ye, J.-J. Xu and H.-Y. Chen, Two-photon excitation nanoparticles for photodynamic therapy, *Chem. Soc. Rev.*, 2016, **45**, 6725–6741.

50 H.-L. Tu, Y.-S. Lin, Y. Hung, L.-W. Lo, Y.-F. Chen and C.-Y. Mou, In vitro Studies of Functionalized Mesoporous Silica Nanoparticles for Photodynamic Therapy, *Adv. Mater.*, 2009, **21**, 172–174.

51 S.-H. Cheng, C.-H. Lee, C.-S. Yang, F.-G. Tseng, C.-Y. Mou and L.-W. Lo, Mesoporous silica nanoparticles functionalized with an oxygen-sensing probe for cell photodynamic therapy: potential cancer theranostics, *J. Mater. Chem.*, 2009, **19**, 1252–1257.

52 D. Brevet, M. Gary-Bobo, L. Raehm, S. Richeter, O. Hocine, K. Amro, B. Loock, P. Couleaud, C. Frochot, A. Morere, P. Maillard, M. Garcia and J. O. Durand, Mannose-targeted mesoporous silica nanoparticles for photodynamic therapy, *Chem. Commun.*, 2009, 1475–1477.

53 S.-H. Cheng, C.-H. Lee, M.-C. Chen, J. S. Souris, F.-G. Tseng, C.-S. Yang, C.-Y. Mou, C.-T. Chen and L.-W. Lo, Trifunctionalization of mesoporous silica nanoparticles for comprehensive cancer theranostics-the trio of imaging, targeting and therapy, *J. Mater. Chem.*, 2010, **20**, 6149–6157.

54 S. H. Hong and Y. Choi, Mesoporous silica-based nanoplatforms for the delivery of photodynamic therapy agents, *J. Pharm. Invest.*, 2018, **48**, 3–17.

55 W. R. Wilson and M. P. Hay, Targeting hypoxia in cancer therapy, *Nat. Rev. Cancer*, 2011, **11**, 393.

56 J. Kim, H. R. Cho, H. Jeon, D. Kim, C. Song, N. Lee, S. H. Choi and T. Hyeon, Continuous O2-Evolving MnFe2O4 Nanoparticle-Anchored Mesoporous Silica Nanoparticles for Efficient Photodynamic Therapy in Hypoxic Cancer, *J. Am. Chem. Soc.*, 2017, **139**, 10992–10995.

57 M. Rizzi, S. Tonello, B. M. Estevao, E. Gianotti, L. Marchese and F. Reno, Verteporfin based silica nanoparticle for in vitro selective inhibition of human highly invasive melanoma cell proliferation, *J. Photochem. Photobiol., B*, 2017, **167**, 1–6.

58 R. C. H. Wong, S. Y. S. Chow, S. Zhao, W.-P. Fong, D. K. P. Ng and P.-C. Lo, pH-Responsive Dimeric Zinc(II) Phthalocyanine in Mesoporous Silica Nanoparticles as an Activatable Nanophotosensitizing System for Photodynamic Therapy, *ACS Appl. Mater. Interfaces*, 2017, **9**, 23487–23496.

59 F. Yuan, J.-L. Li, H. Cheng, X. Zeng and X.-Z. Zhang, A redox-responsive mesoporous silica based nanoplatform for in vitro tumor-specific fluorescence imaging and enhanced photodynamic therapy, *Biomater. Sci.*, 2018, **6**, 96–100.

60 I. Miletto, A. Fraccarollo, N. Barbero, C. Barolo, M. Cossi, L. Marchese and E. Gianotti, Mesoporous silica nanoparticles incorporating squaraine-based photosensitizers: a combined experimental and computational approach, *Dalton Trans.*, 2018, **47**, 3038–3046.

61 G. Chen, H. Qiu, P. N. Prasad and X. Chen, Upconversion Nanoparticles: Design, Nanochemistry, and Applications in Theranostics, *Chem. Rev.*, 2014, **114**, 5161–5214.

62 R. Han, J. Shi, Z. Liu, H. Wang and Y. Wang, Fabrication of Mesoporous-Silica-Coated Upconverting Nanoparticles with Ultrafast Photosensitizer Loading and 808 nm NIR-Light-Triggering Capability for Photodynamic Therapy, *Chem. – Asian J.*, 2017, **12**, 2197–2201.

63 H. Wang, X. Zhu, R. Han, X. Wang, L. Yang and Y. Wang, Near-infrared light activated photodynamic therapy of THP-1 macrophages based on core-shell structured upconversion nanoparticles, *Microporous Mesoporous Mater.*, 2017, **239**, 78–85.

64 S. Kuk, B. I. Lee, J. S. Lee and C. B. Park, Rattle-Structured Upconversion Nanoparticles for Near-IR-Induced Suppression of Alzheimer's β-Amyloid Aggregation, *Small*, 2017, **13**, 1603139.

65 F. Xu, M. Hu, C. Liu and S. K. Choi, Yolk-structured multifunctional up-conversion nanoparticles for synergistic photodynamic-sonodynamic antibacterial resistance therapy, *Biomater. Sci.*, 2017, **5**, 678–685.

66 J. Xu, P. Yang, M. Sun, H. Bi, B. Liu, D. Yang, S. Gai, F. He and J. Lin, Highly Emissive Dye-Sensitized Upconversion Nanostructure for Dual-Photosensitizer Photodynamic Therapy and Bioimaging, *ACS Nano*, 2017, **11**, 4133–4144.

67 T. Zhang, S. Huang, H. Lin, N. An, R. Tong, Y. Chen, Y. Wang and F. Qu, Enzyme and pH-responsive nanovehicles for intracellular drug release and photodynamic therapy, *New J. Chem.*, 2017, **41**, 2468–2478.

68 J. Wang, Y. Li, R. Mao, Y. Wang, X. Yan and J. Liu, Persistent luminescent nanoparticles as energy mediators for enhanced photodynamic therapy with fractionated irradiation, *J. Mater. Chem. B*, 2017, **5**, 5793–5805.

69 H. Chen, X. Sun, G. D. Wang, K. Nagata, Z. Hao, A. Wang, Z. Li, J. Xie and B. Shen, LiGa5O8:Cr-based theranostic nanoparticles for imaging-guided X-ray induced photodynamic therapy of deep-seated tumors, *Mater. Horiz.*, 2017, **4**, 1092–1101.

70 S. H. Hong, H. Kim and Y. Choi, Enhanced Fluorescence Imaging and Photodynamic Cancer Therapy Using Hollow Mesoporous Nanocontainers, *Chem. – Asian J.*, 2017, **12**, 1700–1703.

71 H. Suk ho, K. Hyunjin and C. Yongdoo, Indocyanine green-loaded hollow mesoporous silica nanoparticles as an activatable theranostic agent, *Nanotechnology*, 2017, **28**, 185102.

72 Y. Kuthati, R. K. Kankala, P. Busa, S.-X. Lin, J.-P. Deng, C.-Y. Mou and C.-H. Lee, Phototherapeutic spectrum expansion through synergistic effect of mesoporous silica trio-nanohybrids against antibiotic-resistant Gram-negative bacterium, *J. Photochem. Photobiol., B*, 2017, **169**, 124–133.

73 P. L. Abbaraju, Y. Yang, M. Yu, J. Fu, C. Xu and C. Yu, Core–Shell-structured Dendritic Mesoporous Silica Nanoparticles for Combined Photodynamic Therapy and Antibody Delivery, *Chem. – Asian J.*, 2017, **12**, 1465–1469.

74 R. Tong, H. Lin, Y. Chen, N. An, G. Wang, X. Pan and F. Qu, Near-infrared mediated chemo/photodynamic synergistic therapy with DOX-UCNPs@mSiO2/TiO2-TC nanocomposite, *Mater. Sci. Eng., C*, 2017, **78**, 998–1005.

75 Y. Liu, X. Liu, Y. Xiao, F. Chen and F. Xiao, A multifunctional nanoplatform based on mesoporous silica nanoparticles for imaging-guided chemo/photodynamic synergetic therapy, *RSC Adv.*, 2017, **7**, 31133–31141.

76 W.-H. Chen, G.-F. Luo, W.-X. Qiu, Q. Lei, L.-H. Liu, S.-B. Wang and X.-Z. Zhang, Mesoporous silica-based versatile theranostic nanoplatform constructed by layer-by-layer assembly for excellent photodynamic/chemo therapy, *Biomaterials*, 2017, **117**, 54–65.

77 R. C. H. Wong, D. K. P. Ng, W. P. Fong and P. C. Lo, Encapsulating pH-Responsive Doxorubicin–Phthalocyanine Conjugates in Mesoporous Silica Nanoparticles for Combined Photodynamic Therapy and Controlled Chemotherapy, *Chem. – Eur. J.*, 2017, **23**, 16505–16515.

78 J. Liu, D. Sen Karaman, J. Zhang, J. M. Rosenholm, X. Guo and K. Cai, NIR light-activated dual-modality cancer therapy mediated by photochemical internalization of porous nanocarriers with tethered lipid bilayers, *J. Mater. Chem. B*, 2017, **5**, 8289–8298.

79 C. Shiqiang, G. Yu, Z. Zhenyu, C. Zhen, M. Yurong and Q. Limin, Cyclodextrin-gated mesoporous silica nanoparticles as drug carriers for red light-induced drug release, *Nanotechnology*, 2017, **28**, 145101.

80 T. Yan, J. Cheng, Z. Liu, F. Cheng, X. Wei and J. He, pH-Sensitive mesoporous silica nanoparticles for chemo-photodynamic combination therapy, *Colloids Surf., B*, 2018, **161**, 442–448.

81 H. Yang, Y. Chen, Z. Chen, Y. Geng, X. Xie, X. Shen, T. Li, S. Li, C. Wu and Y. Liu, Chemo-photodynamic combined gene therapy and dual-modal cancer imaging achieved by pH-responsive alginate/chitosan multilayer-modified magnetic mesoporous silica nanocomposites, *Biomater. Sci.*, 2017, **5**, 1001–1013.

82 G. Liu, J. Ma, Y. Li, Q. Li, C. Tan, H. Song, S. Cai, D. Chen, Z. Hou, Q. Chen and X. Zhu, Core-interlayer-shell Fe3O4@mSiO2@lipid-PEG-methotrexate nanoparticle for multimodal imaging and multistage targeted chemo-photodynamic therapy, *Int. J. Pharm.*, 2017, **521**(1–2), 19–32.

83 Y. Jang, S. Kim, S. Lee, C.-M. Yoon, I. Lee and J. Jang, Graphene Oxide Wrapped SiO2/TiO2 Hollow Nanoparticles Loaded with Photosensitizer for Photothermal and Photodynamic Combination Therapy, *Chem. – Eur. J.*, 2017, **23**, 3719–3727.

84 Q. Sun, Q. You, X. Pang, X. Tan, J. Wang, L. Liu, F. Guo, F. Tan and N. Li, A photoresponsive and rod-shape nanocarrier: Single wavelength of light triggered photothermal and photodynamic therapy based on AuNRs-capped & Ce6-doped mesoporous silica nanorods, *Biomaterials*, 2017, **122**, 188–200.

85 S. Goel, C. A. Ferreira, F. Chen, P. A. Ellison, C. M. Siamof, T. E. Barnhart and W. Cai, Activatable Hybrid Nanotheranostics for Tetramodal Imaging and Synergistic Photothermal/Photodynamic Therapy, *Adv. Mater.*, 2018, **30**(6), 1704367.

86 Y. Chen, F. Zhang, Q. Wang, R. Tong, H. Lin and F. Qu, Near-infrared light-mediated LA-UCNPs@SiO2-C/HA@mSiO2-DOX@NB nanocomposite for chemotherapy/PDT/PTT and imaging, *Dalton Trans.*, 2017, **46**, 14293–14300.

87 Y. Wang, G. Yang, Y. Wang, Y. Zhao, H. Jiang, Y. Han and P. Yang, Multiple imaging and excellent anticancer efficiency of an upconverting nanocarrier mediated by single near infrared light, *Nanoscale*, 2017, **9**, 4759–4769.

88 S. Fang, J. Lin, C. Li, P. Huang, W. Hou, C. Zhang, J. Liu, S. Huang, Y. Luo, W. Fan, D. Cui, Y. Xu and Z. Li, Dual-Stimuli Responsive Nanotheranostics for Multimodal Imaging Guided Trimodal Synergistic Therapy, *Small*, 2017, **13**(6), 1602580.

89 Q. Sun, Q. You, J. Wang, L. Liu, Y. Wang, Y. Song, Y. Cheng, S. Wang, F. Tan and N. Li, Theranostic Nanoplatform: Triple-Modal Imaging-Guided Synergistic Cancer Therapy Based on Liposome-Conjugated Mesoporous Silica Nanoparticles, *ACS Appl. Mater. Interfaces*, 2018, **10**, 1963–1975.

